This file mainly consists of three parts. The first one is the point-by-point response to the comment of three referees. The second one is a list of all relevant changes made in the manuscript. The third one is the revised manuscript, in which the relevant change was marked up with yellow.

Response to Anonymous Referee #1

General comments

The paper deals with debris-flow occurrence thresholds in terms of rainfall intensity-duration by using radar data in an earthquake-affected area (Sichuan, China). The paper addresses technical questions within the scope of NHESS and is conform to international standards; scientific methods are clearly outlined. Authors try to address the definition of the rainfall-field by the use of radar to better evaluate the relation between rainfall and debris-flow. But, as described in the technical comments, to overcome some objective limitations of the methodology used, further investigations would be needed to properly take into account the susceptibility of the territory. The title is clear; the abstract is pertinent, easy to understand and resumes well the contents of the paper. Mathematical formulas, symbols and abbreviations are correctly defined. Technical language is precise and understandable.

An I-D threshold curve is proposed on the basis of six rain events that caused 512 debris-flows between 2012 and 2014. Based on rain data estimates obtained from 2 radars, the authors use various techniques for estimating rainfall from reflectivity, by also considering the rainfall detected by rain gauges for comparative analysis and correction of the bias. As shown, the use of radar data provides a better estimate of the precipitations responsible of landslides triggering. In one case (cf. Table 2), the amount of rain measured by radar is 10 times greater than that detected by the rain gauge network (Event # 3). Before evaluating the I-D threshold, the authors describe some techniques to detect the best estimate of radar precipitation, identifying the Kalman's filtering application as the best tool to reduce radar-rain gauge bias. Using the frequentist approach, the authors compute the relation $I = \alpha D^{-\beta}$ which binds intensity and duration of precipitation for three estimates of rainfall fields. Scatter plots are shown in fig. 8

Response: We sincerely thank the reviewer for giving so helpful suggestions. In this paper we try to evaluate the feasibility and limitation for radar-based regional I-D thresholds over earthquake affected area in China. The information on hydrology, lithology, land use, geomorphology over study area could enhance the understanding of debris flow initiation. Some information on underlying surface are provided in the following paragraph describing the response. However doing an in-depth delving into those topics is beyond the scope of this paper.

Technical Comments

The article is of interest as it performs a radar application on I-D threshold models, historically developed using only rain gauges. Although, I-D thresholds generally suffer from limitations that can affect practical applications. In fact, in case of convective rainfall events (responsible of most debris-flow and shallow-landslide events), the area affected by ground effects is usually small (normally few km2) and tends to reproduce a low I-D curve when only rain gauges are used. On the other hand, landslides occur in correspondence of highest rainfall intensities. Aiming at evaluating the precipitation field, authors try to solve the problem by also using radar data, and considering possible estimation errors. Another intrinsic lack of the

method lies in the determination of the duration of the event, and the simplification of the average intensity or accumulated precipitation for the whole interval. Analyses of uniform rainfall distribution inside the intervals excludes soil characteristics that heavily affect the development of gravitational movements. In the case of stratiform rain events, with uniform intensity, landslides are more frequent in permeable areas; in case of convective rainfalls, landslides are more easily triggered in areas with low permeability. An additional limit of the model is the absence of discriminant analysis of susceptibility to shallow landslides in the study area. The adopted method for determining the threshold I-D, in fact, ignores lithology, geomorphology (e.g. slope), land use, and soil coverage. Consequently, it tends to lower the threshold as is results mostly controlled by the most fragile portions of the territory. Looking at the threshold I-D of Figure 8 for the same duration of precipitation, the corresponding rain intensity that triggers debris-flow varies with one order of magnitude. The paper, assessing thresholds I-D using radar rainfall field, contributes to improve the model by reducing limitations due to the use of only rain gauges, especially in the case of convective phenomena. Among possible improvements to the method, multiple thresholds (e.g. for class of slope, lithology, etc.) could be considered in addition to accurate rainfall radarestimation.

Response: We thank the reviewer for the valuable and constructive comment. We totally agree with the reviewer that the detailed spatial information on the hydrological, lithological, morphological, and soil characteristics could help us better understand the physical initiation of shallow landslides. In the revision, we have added the information about lithology, land use and morphology. In addition, potential debris flow watersheds are retrieved. We have updated the manuscript to include these points (P3L27). However, we want to note that it is challenging to get the high resolution high quality data continuously for this area, such as soil water status and soil drainage. Therefore, the empirical model is adopted in this study. The manuscript was supplemented with the following contents:

"The geological structure of the study area show a northeast to southwest orientation. The rocks over this region are mainly comprised of volcanic rocks, mixed sedimentary rocks, siliciclastic sedimentary rocks, carbonate sedimentary rocks, acid plutonic rocks, intermediate colcanic rocks, intermediate plutonic rocks, unconsolidated sediments, metamorphic rocks, basic Plutonic Rocks, and pyroclastic rocks. Figure 1a shows the lithological map. Quaternary deposits were distributed in the form of river terraces and alluvial fans. Owing to frequent tectonic activities, most of the gully are steeply sloped over this area. The main land use types in this region are mixed forest, cropland, and grassland, as shown in Figure 1b."(P.3 L.27)

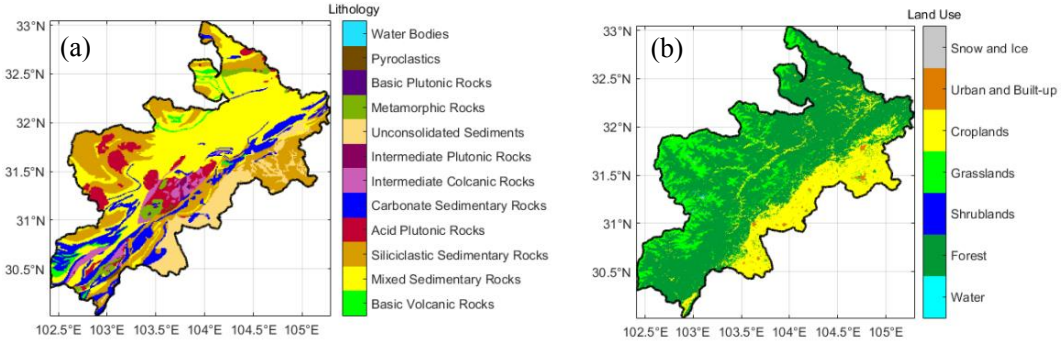

Figure 1. Lithology map (a) and land use map (b) for the study area

“Potential DF watersheds over study area is extracted from morphological variables, using the logistic regression method. Berenguer et al.(2015) simplified the geomorphological variables, as the watersheds maximum height(h_{max}), mean slope(s_{mean}), mean aspect(θ_{mean}) and melton ratio(MR) are the variables with the smallest overlapping areas for assessing the susceptibility of the watersheds. The h_{max}, s_{mean}, θ_{mean} and MR were retrieved from DEM data. Combined with the DF occurrence over this area in the three years, the potential susceptibility map was calculated with logarithm regression method as shown in the figure 2c. “(P.4,L.2)

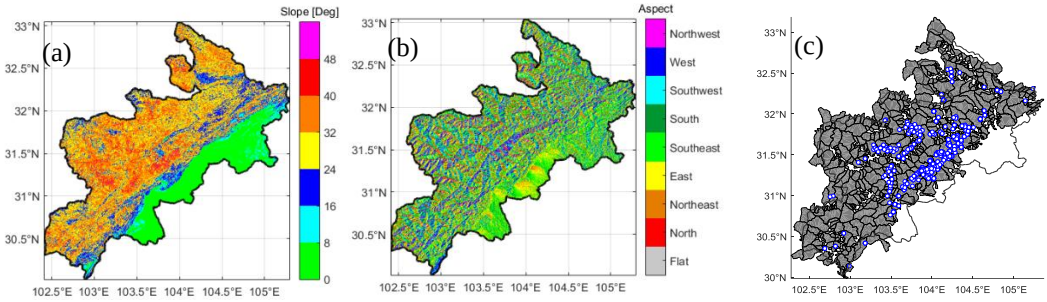

Figure 2. Morphology and potential DF watersheds map over study area.(a) slope, (b) aspect, (c) potential DF watersheds(gray polygon) with DF observation(blue circle)

“The identification results show that there are 673 potential debris flow watersheds in this region. 519 debris flows triggered by six rainfall events (point data) are shown in Figure 2c. In total, 98.6 % of the identified DF watersheds are located in the potential DF watersheds. “

Concerning the empirical relation of rainfall and debris flow, we adopted the widely used model described in (Guzzetti et al., 2007) , as D here is the duration from the beginning of the rainfall to the occurrence of the debris flow (h), and I is the mean rainfall intensity in the period of D (mm h^{-1}). The duration and intensity are determined by an interval of at least 24 hours, rain rates of less than 0.1 mm h^{-1}, or correspondingly radar reflectivity of less than 10 dBz to separate two consecutive rainfall events. We also note that there are various definition of rainfall thresholds for the initiation of debris flow in lots of literatures. Based on reviewer’s constructive comment, we also would like go further to apply those definitions and investigate its performance in the following study by using the radar data.

In a word, we sincerely thank the reviewer for giving us so insightful comments and constructive suggestions.

Reference:

Guzzetti, F., Peruccacci, S., Rossi, M., and Stark, C. P.: Rainfall thresholds for the initiation of landslides in central and southern Europe, Meteorology and atmospheric physics, 98, 239-267, 2007.

M. Berenguer, D. Sempere-Torres, and M. Hürlimann.: Debris-flow forecasting at regional scale by combining susceptibility mapping and radar rainfall.Nat. Hazards Earth Syst. Sci., 15, 587–602,2015.

Response to Anonymous Referee #2

General Comments: This manuscript investigates the debris flow occurrence using rainfall Intensity-Duration (I-D) information in the earthquake-affected areas in Sichuan, China. Two S-band Doppler radars are used to estimate rainfall in the study domain characterized by complex terrain. Therein, traditional Z-R relations are adopted with additional attention paid to vertical profile of reflectivity (VPR) correction and Kalman filter based bias correction. The I-D curves are then calculated using a frequentist approach with the radar derived rainfall products.

Response: We sincerely thank the reviewer for valuable and constructive suggestions. The followings are our responses to the reviewer.

Overall, this topic well fits the scope of NHESS. The methodology used in the paper is scientifically sound. The study shows several valuable scientific results, which can possibly be used for guidance of debris flow warnings. Nevertheless, some minor changes will improve paper clarity. Specific comments are listed below:

1. The writing needs to be improved. Please proofread the manuscript before submitting the revised version. Specific examples of mistakes are presented below: 1.1. Page 2, Line 15: highly rely-> highly relies 1.2. Page 3, Line 1: have to be -> has to be 1.3. Page 25, caption of Figure 7: event->events 1.4. Page 26, caption of Figure 8: possibility->probability

   Response: We thank the reviewer for the careful revision. Those were changed as suggested.

2. Reference formatting should be more consistent throughout the manuscript. There are numerous references that are not cited in correct form. For examples, Qiang W. et al., 2015; Xiaojun G. et al 2016; Michele C. et al., 2015; Francesco M. et al., 2014; and many others.

   Additional Related Reference: Willie, D., H. Chen, and V. Chandrasekar, et al., 2017: Evaluation of Multisensor Quantitative Precipitation Estimation in Russian River Basin. Journal of Hydrologic Engineering, 22(5), E5016002, doi: 10.1061/(ASCE)HE.1943- 5584.0001422.

   Response: We thank the reviewer for pointing this out. The references are reformatted in accordance with Endnote template of Copernicus Publications. This reference suggested by reviewer also emphasized the combination of using radar and rain gauges to provide accurate rainfall estimates in complex terrain. It shows the necessity of radar-based rainfall estimation for improving warnings of future precipitation and situational awareness. We referred this article in the revision. (P.3,L4)

3. Page 2, Line 14: Early Warning System Using acronym would be enough since it had been mentioned earlier.

   Response:Totally Agree! The acronym is used as suggested.

4. Page 4, Line 5: performance specifications->system specifications

   Response: We thank the reviewer for pointing this out. Totally agree. Changed as suggested.

5. Page 5, Lines 14-16: The authors are using different tilt data trying to obtain rainfall estimates at the same vertical level. What is the purpose of doing this? Getting rainfall closer to surface might be more useful (provided that lowest level data is not blocked).

Response: We thank the reviewer for this comment. We agree the idea of getting rainfall closer to surface with the reviewer. However, in our study, the hybrid mode using multiple elevation is not only to get the rainfall closer to surface for complex terrain, but also used to align the radar data from same altitude for the flat area where dense rain gauge are deployed. This manner here is expected to decrease the uncertainty of altitude factor (earth curvature) for correction using rain gauge. For sure, it might be more useful to get rainfall closer to surface, if radar bias and rainfall microphysics are well understood.

6. Page 6, Line 23: The rationale of using these two Z-R relations is insufficient. It is well known that Z-R is greatly dependent on local rainfall microphysics. A local DSD- based variability analysis would be helpful.

   Response: We thanks the reviewer for this constructive suggestion. The DSD observation and microphysics retrieval has been proven beneficial to improve the accuracy of radar-based rainfall estimate, however, the DSD observations are rarely scarce for study area. It's believed that building the composite rainfall observing network will improve the QPE accuracy, furthermore enhance the performance of EWS.

7. Page 15, Table 1: doppler->Doppler

   Response: Totally Agree! Changed as suggested!

8. Page 15, Table 1: The pulse width seems not matching with the range resolution. Please clarify.

   Response: We thank the reviewer for this detailed check. The original transmitted pulse is 1μs, while the final filed variables are averaged within two range gates, which is pre-defined operational mode and cannot be changed by data user. Therefore, the range resolution is decreased from 150m to 300m. To avoid the misunderstanding for reader, the item of transmitted pulse will be remove from the table 1.

Response to Anonymous Referee #3

The manuscript presents an analysis of rainfall intensity-duration (I-D) thresholds used for the identification of debris-flow occurrence. Estimation of gauge and radar-based I- D threshold is carried out and compared. The work in this manuscript is very similar to the one carried out by Marra et al. 2014 thus from a methodological point of view there is no significant novelty. However, the authors carry out the analysis in a completely different region with different hydroclimatic characteristics and as such I consider the results to be complementary to what we already know from past studies. Therefore, I consider overall that the results reported in this work add to our knowledge and further highlight the significance of using remote sensing observations for the estimation of debris flow triggering rainfall. I am including below a list of comments/suggestions that can hopefully help the authors to improve their manuscript.

We sincerely thank the reviewer for giving us so valuable and constructive suggestions. The followings are our responses to the reviewer.

1. Page 4, L11-25: This last paragraph should be placed in a different section (not the study area and data). You could have a dedicated section to discuss event characteristics. Also in that same paragraph, you mention info that relates to methodology (e.g. identification of individual rainfall event) that should be placed in the methodology section.

   Response: We thank the reviewer for this helpful suggestion. The contents of this paragraph are adjusted according to this comment. Those contents related to event characteristic and identification of individual rainfall event were moved to the section 4 in the revision.(P8L22-P9L7)

2. Provide a more detailed analysis of the comparison between radar rainfall estimates at DF (debris flow location) and closest-gauge estimates. For example, a graph showing relative error (y-axis) vs distance (between closest gauge and DF) would be informative. Using different colors per event (on such a graph) would also provide some more info. Lastly, it would be interesting to show that for both rainfall intensity and duration, since you are reporting differences in duration as well. Differences in duration, although important for building I-D thresholds, are not frequently explored. I believe adding some more info on this would strengthen the overall analysis.

   Response: We thank the reviewer for the valuable and instructive suggestion. Based on this constructive comment, we added a new subsection 4.3 of 'Impact of rainfall spatial variation on Intensity and Duration'

   The accumulated rainfall, duration and rainfall intensity identified from the nearest rain gauge probably are different from the realities occurred at the debris flow location, since the rainfall varies in space especially for convective precipitation with sharp variation in short distance. The observed rainfall differences rely on the distance from the nearest rain gauge to the debris location and could be considered as spatial errors. To this end, relative errors of the accumulated rainfall, duration, and rainfall intensity versus distance are calculated from the comparisons with the radar-based estimate at the location of debris flow. The metrics for evaluating relative error versus distance are defined in the following table (Table 5 in the revision). There are also some predefined conditions for the comparison of relative errors versus distance: (1) The radar rainfall estimation used for comparison are all from scenario III. (2) The radar rainfall estimation and duration identification at the debris flow location are considered as the true referred value. (3) The maximum distance from debris

flow location to the nearest rain gauge is predefined within 10 km and the distance resolution is set equal to those two CINRADs' range resolution of 300 meters. (4) In order to assess the rainfall spatial variation using multi-sensor, the radar-based estimate at the co-location of the nearest rain gauge, as well as rain gauge observation, is also compared with the radar-based estimate at the location of debris flow.

Table 1. The metric for assessing the relative errors of the accumulated rainfall, duration and rainfall intensity versus distance

Factors	Rain gauge observation nearest to DF location versus Radar estimate at DF location	Radar estimate at the co-location of rain gauge versus Radar estimate at DF location
Accumulated Rainfall Relative Error (ARRE)	$ARRE_g(s) = \frac{\sum_{i=1}^{N(s)} \lvert R_{df}(i) - R_g(i) \rvert}{\sum_{i=1}^{N(s)} R_{df}(i)} \times 100\%$	$ARRE_r(s) = \frac{\sum_{i=1}^{N(s)} \lvert R_{df}(i) - R_r(i) \rvert}{\sum_{i=1}^{N(s)} R_{df}(i)} \times 100\%$
Duration Relative Error (DRE)	$DRE_g(s) = \frac{\sum_{i=1}^{N(s)} \lvert D_{df}(i) - D_g(i) \rvert}{\sum_{i=1}^{N(s)} D_{df}(i)} \times 100\%$	$DRE_r(s) = \frac{\sum_{i=1}^{N(s)} \lvert D_{df}(i) - D_r(i) \rvert}{\sum_{i=1}^{N(s)} D_{df}(i)} \times 100\%$
Rainfall Intensity Relative Error (RIRE)	$RIRE_g(s) = \frac{\sum_{i=1}^{N(s)} \lvert I_{df}(i) - I_g(i) \rvert}{\sum_{i=1}^{N(s)} I_{df}(i)} \times 100\%$	$RIRE_r(s) = \frac{\sum_{i=1}^{N(s)} \lvert I_{df}(i) - I_r(i) \rvert}{\sum_{i=1}^{N(s)} I_{df}(i)} \times 100\%$

Note. *R* represents accumulated rainfall for debris flow event, *D* represents duration for rainfall event, *I* represents the mean intensity for rainfall event. The variables with subscript df, g and r respectively represent the observation from radar at debris flow location, rain gauge nearest to debris flow location, and radar at the co-location of the nearest rain gauge. s represents the distance between the nearest rain gauge location and debris flow location with the range resolution of 300m. N(*s*) represent the number of rain gauge observation for debris flow at the distance of *s*.

The metrics of Accumulated Rainfall Relative Error (ARRE), Duration Relative Error (DRE) and Rainfall Intensity Relative Error (RIRE) are calculated for the nearest rain gauge and radar estimate at the co-location respectively. The results of ARRE, DRE and RIRE versus distance are drawn in the following Figure (Figure 13 in the revision). The main findings from the evaluation results are summarized as follows:

(1) The results of ARRE, DRE and RIRE all have an enlarging tendency along with the increasing distance. The maximum ARRE, DRE and RIRE for rain gauge observation is 42.2%, 41.67% and 55.88%, respectively. The maximum ARRE, DRE and RIRE for radar-based estimate at the co-location of the nearest rain gauge is 43.33%, 41% and 45.2%, respectively.

(2) Nonlinear regression is applied for ARRE, DRE and RIRE versus distance to investigate the average tendency, as shown in the following figure (Figure 13 in the revision). The regression curves of ARRE and DRE for rain gauge and

radar are approximately similar within 10km and 4km, respectively, indicating radar estimate and rain gauge observation have the similar rainfall spatial variation impacts.

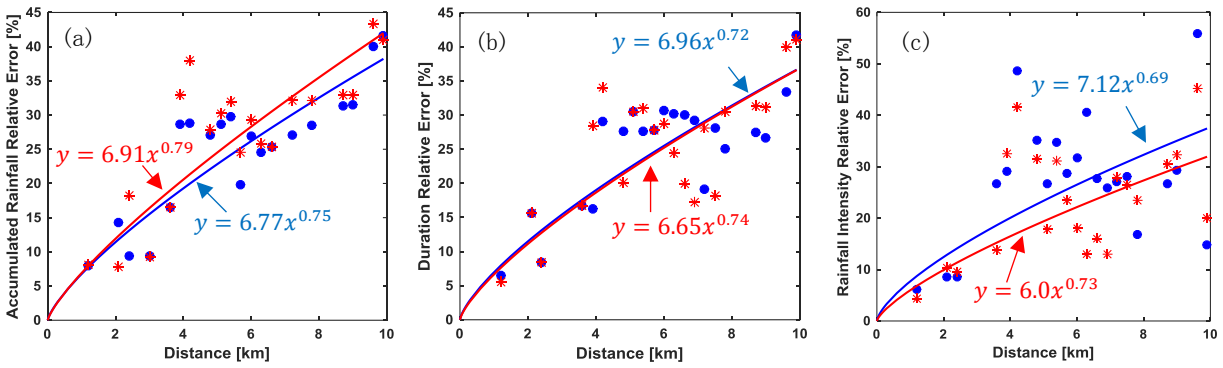

Figure 1. Scatterplot of relative errors versus distance. Blue circle dot represent relative error between radar estimate at debris flow location and rain gauge observation closest to debris flow location. Red asterisk represent relative error between radar estimate at debris flow location and radar estimate at the position of closet rain gauge.(a) Accumulated Rainfall Relative Error, (b) Duration Relative Error, (c) Rainfall Intensity Relative Error.

We clarified those in the new section 4.3 in the revision.(P11L18-P12L7)

We were also inspired by the reviewer's excellent suggestion of using different colors per event (on such a graph). As far as the events in this study are concerned, we found there were not sufficient samples to estimate the statistical relation between relative error and distance for separate event 1, 2, 4 and 6, which would lead to incomparable for those events. We decided not to compare relative error versus distance for individual event. However, we were deeply impressed by this suggestion, and would collect more eligible events for further study.

3. Provide also quantification metrics for changes in I-D parameters (α and β).

Response: We thank the reviewer for this suggestion. We further take the α and β estimated from Scenario III as the right referred value, and calculate the relative error of α and β for each scenario, as shown in the following table (table 6 in the revision). The relative error of α for Scenario I, II, and III is -24.5%, -13.8% and 0%, respectively. The relative error of β for Scenario I, II, and III is -28.8%, -17.3% and 0%, respectively. It is indicated that improving the accuracy of rainfall estimate is able to decrease the relative errors of α and β, Considering rainfall spatial variation, the relative error of α for the nearest gauge observation and radar-based estimate at the co-location is -49.5% and -42.6%, respectively. The relative error of β for the nearest gauge observation and radar-based estimate at the co-location is -19.5% and -21.2%, respectively. The relative error of α is remarkably larger than the one derived from radar-based estimate at the debris flow location,

however, the differences of α and β for rain gauges and radar-based estimate at the co-location are not significant. We clarified those in the section 4.3 of revision.(P12L8-17)

Table 2. Parameters of the identified ID thresholds and relative errors

	α	$\frac{\alpha - \alpha_{S3}}{\alpha_{S3}} \times 100\%$	β	$\frac{\beta - \beta_{S3}}{\beta_{S3}} \times 100\%$
Scenario I	7.62	-24.5	0.67	28.8
Scenario II	8.7	-13.8	0.43	-17.3
Scenario III	10.1	0.0	0.52	0.0
Rain gauges	5.1	-49.5	0.42	-19.2
Radar estimate at the co-location of the nearest rain gauge	5.8	-42.6	0.41	-21.2

Note. α_{S3}, β_{S3} here equals to α, β estimated from Scenario III, respectively.

4. A professional or native English speaker needs to carefully edit the manuscript for grammatical errors and inappropriate wording (e.g. p10L1 “effectivity” p10L7 “induce” etc)

   Response: We thank the reviewer for this good suggestion. The whole manuscript were read and revised by native English speaker.

5. P5L3: “ensure the rainfall estimation accuracy” is quite a strong statement. Please revise.

   Response: We thank the reviewer for pointing this out. Totally agree! The aim of processing is to improve the rainfall estimation accuracy, the sentence is revised as “improve the rainfall estimation accuracy”.(P4L31)

6. P5,L27: Define VIL

   Response: We thank the reviewer for pointing this out. The definition of Vertically Integrated Liquid (VIL) is added in the manuscript as “To discriminate convection precipitation from stratiform based on the composite reflectivity>50dBz or VIL >6.5 kg/m2, where VIL is acronym of Vertically Integrated Liquid water content and it is an estimate of the total mass of precipitation in the clouds. (Amburn and Wolf, 1997)” (P5L24)

7. P5,L31-32: “It can be seen that . . .rely on temperature, air dynamic . . .”. I don’t think that these can be seen from Figure 4 alone. Please revise.

   Respone: We thank the reviewer for pointing this out. We clarified this in the revision as” Impacted by the temperature, air dynamic, particle size and phase are changed along the vertical falling. Figure 5 shows vertical profile of reflectivity varied approximately as three piecewise linear sections”.(P5L29)

8. Do you have any justification for the choice of 1.5km as the height threshold for separating the two regions?

   Response: The reason of separating two region is the vertical variation of rainfall rate profile, especially for convective rainfall. Normally, the low scanning elevation PPI is used to estimate ground rainfall rate. Considering the limitation of scanning elevation, station height, and earth curvature, the height from flat terrain is nearly 1.5 km if the radial range is

100 km (normally under maximum detection range) away from radar, even for the lowest elevation of 0.5°. Concerning complex terrain of study area, the elevation almost has to be uplifted to avoid beam blockage when radial distance is over 100 km. Therefore, 1.5 km is set as height threshold for this study to discriminate where is closer to ground and where is higher from ground. The following figure briefly illustrate the radar beam locating height along the radial distance.

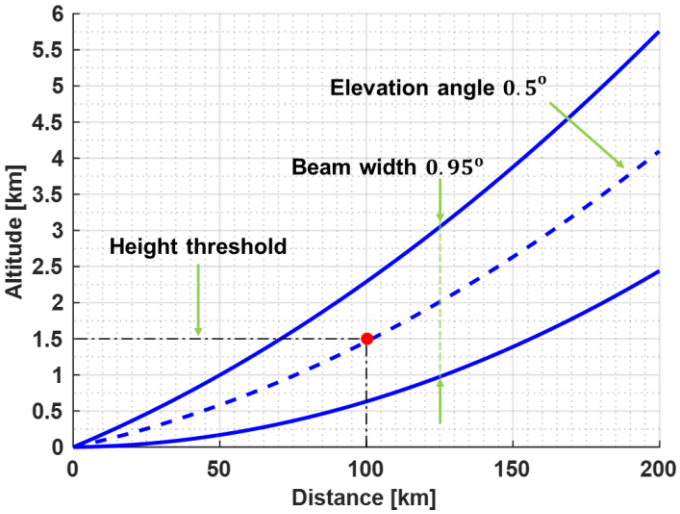

Figure 2. Radar beam locating height along the radial distance

9. P7L24: "between each hour is tiny" perhaps should be "within each hour is negligible". Please check and revise accordingly

   Response: We thank the reviewer for this revision. Changed as suggested. This sentence will be revised in the manuscript as "It is assumed that the variation of the real bias within each hour is negligible" (P7L23)

10. P7L25: "so initial conditions of KF are. . ." I don't believe that the exact numbers for Q, S etc are a result of the previously stated assumption. Revise accordingly.

    Response: We thank the reviewer for pointing this out. This sentence is revised as "the initial estimator for mean field radar rainfall logarithmic bias and it's error variance are assumed to equal their update values which are respectively the $BIAS_{KF}(0)$ and $P_{KF}(0)$.(P7L23)

11. Be consistent with the reporting of equations. Some are in text instead of being numbered as others. Also in P8,L9, you should write log[If(D)] instead of log(I). Revise also the sentence stating "β here accounting for nearly 50% occurrence probability. . .". It is the intercept, not the exponent that relates to the probability according to the frequentist approach you used.

    Response: Totally agree! log[If(D)] is written instead of log(I) in P8,L9. The modification is made as "where α_{50} , β is the fitted intercept and slope, respectively".(P8L6)

12. P9,L1 and elsewhere: use "scenarios" instead of "scene"

Response: We thank the reviewer for pointing this out. Totally agree! Changed as suggested. All of "scene" are replaced with "scenarios" in the revision.

13. 13. Equations 14 and 15 have the same formula. Please revise

    Response: Equation 14 is normalized standard error (NSE), equation 15 is normalized mean bias (NMB).We clarified those equations in the revision as suggested.

14. Define what do you mean by "linear ratio".

    Response: The linear ratio is the slope estimated from linear regression of radar rainfall estimation and rain gauge observation, with the predefined intercept of zero. The linear ratio here is used to evaluate how much average ratio radar-based rainfall is to the observation of rain gauge. The linear ratio approximates to one, if radar-based rainfall estimation is consistent with rain gauge observation. We clarified this in the revision. (P9L20)

15. P10,L10-11: "The PDF estimations reveal that the number of positive difference δ(D) is more than number of negative difference". I am not sure what the point you are trying to make here is. Also, if you think that the distribution of residuals is asymmetric, then you should not fit a Gaussian distribution. This affects also the frequentist approach you followed. Please revise/clarify this point.

    Response: We thank the reviewer for the comment. Perhaps it was not clear in the writing. But we would like to note that although the distribution of residuals is not strictly symmetric for low probability density, the sole peak and high probability density are conform to Gaussian distribution. The related sentences were eliminated in the revision.

The list of all relevant changes made in the manuscript

NO.	Position in the revision	Changes
1.	P2L14	Revised: Early Warning System-> EWS
2.	P2L15	Revised: rely->relies
3.	P3L1	Revised: have-> has
4.	P3L4	New added content: Therefore, the combination of using radar and rain gauges to provide accurate rainfall estimates in complex terrain attracts increasingly more interest for improving warnings of future precipitation and situational awareness (Willie et al., 2017).
5.	P3L18	Revised: Closest->nearest
6.		All of the term 'scene' are replaced with 'scenario'
7.	P4L18	Revised: performance-> system
8.	P3L27	New added content: The geological structure of the study area show a northeast to southwest orientation. The rocks over this region are mainly comprised of volcanic rocks, mixed sedimentary rocks, siliciclastic sedimentary rocks, carbonate sedimentary rocks, acid plutonic rocks, intermediate colcanic rocks, intermediate plutonic rocks, unconsolidated sediments, metamorphic rocks, basic Plutonic Rocks, and pyroclastic rocks. Figure 1a shows the lithological map. Quaternary deposits were distributed in the form of river terraces and alluvial fans. Owing to frequent tectonic activities, most of the gully are steeply sloped over this area, as shown in the Figure 2a.
9.	P4L1	New added content: The main land use types in this region are mixed forest, cropland, and grassland, as shown in Figure 2b.
10.	P4L2	New added content: Potential DF watersheds over study area were extracted from morphological variables, using the logistic regression method. M. Berenguer(2015) simplified the geomorphological variables, as the watersheds maximum height (h_{max}), mean slope (s_{mean}), mean aspect (θ_{mean}) and melton

		ratio (MR) are the variables with the smallest overlapping areas for assessing the susceptibility of the watersheds. The h_{max}, s_{mean}, θ_{mean} and MR were retrieved from DEM data. Combined with the DF occurrence over this area during the three years, the potential susceptibility map was calculated with logarithm regression method, as shown in the figure 3. The identification results show that there are 673 potential debris flow watersheds in this region.
11.	P4L30	ensure the rainfall estimation accuracy -> improve the rainfall estimation accuracy
12.	P5L24	New added content: where VIL is acronym of Vertically Integrated Liquid water content and it is an estimate of the total mass of precipitation in the clouds (Amburn and Wolf, 1997)
13.	P5L29	Revised: Impacted by the temperature, air dynamic, particle size and phase are changed along the vertical falling. Figure 5 shows vertical profile of reflectivity varied approximately as three piecewise linear sections.
14.	P7L23	Revised: It is assumed that the variation of the real bias within each hour is negligible, the initial estimator for mean field radar rainfall logarithmic bias and its error variance are assumed to equal their update values which are respectively the $BIAS_{KF}(0)$ and $P_{KF}(0)$.
15.	P8L7	Revised: $\log(I_f) = \log(\alpha_{50}) - \beta\log(D)$, where α_{50} , β is the fitted intercept and slope, respectively .
16.	P9L27	New added content: The linear ratio is estimated from linear regression of radar rainfall estimation and rain gauge observation, with the predefined intercept of zero. The linear ratio approximates to one, if radar-based rainfall estimation is consistent with rain gauge observation.
17.	P11L17	New added subsection of 'Impact of rainfall spatial variation on Intensity and Duration'
18.	P14L1	References were reformatted in accordance with Endnote template of Copernicus Publications.

Radar-Based Quantitative Precipitation Estimation for the Identification of Debris-Flow Occurrence over Earthquake affected Region in Sichuan, China

Zhao Shi[1,2,3,5], Fangqiang Wei[1,2,3], Chandrasekar Venkatachalam[4]

[1]Key Laboratory of Mountain Hazards and Earth Surface Process, Chengdu, 610041, China
[2]Institute of Mountain Hazards and Environment, Chinese Academy of Sciences, Chengdu, 610041, China
[3]University of Chinese Academy of Sciences, Beijing, 100049, China
[4]Colorado State University, Fort Collins, 80523, USA
[5]Chengdu University of Information and Technology, Chengdu, 610225, China

Correspondence to: Zhao Shi (shi_zhao@foxmail.com)

Abstract. Both of Ms8.0 Wenchuan earthquake on May 12, 2008 and Ms7.0 Lushan earthquake on April 20, 2013 occurred in Sichuan Province of China. In the earthquake affected mountainous area, a large amount of loose material caused a high occurrence of debris flow during the rainy season. In order to evaluate the rainfall Intensity–Duration (I-D) threshold of the debris flow in the earthquake-affected area, and for filling up the observational gaps caused by the relatively scarce and low altitude deployment of rain gauges in this area, raw data from two S-band China New Generation Doppler weather radar (CINRAD) were captured for six rainfall events which triggered 519 debris flows between 2012 and 2014. Due to the challenges of radar quantitative precipitation estimation (QPE) over mountainous area, a series of improving measures are considered including the hybrid scan mode, the vertical reflectivity profile (VPR) correction, the mosaic of reflectivity, a merged rainfall-reflectivity(R-Z) relationship for convective and stratiform rainfall and rainfall bias adjustment with Kalman filter (KF). For validating rainfall accumulation over complex terrains, the study areas are divided into two kinds of regions by the height threshold of 1.5 km from the ground. Three kinds of radar rainfall estimates are compared with rain gauge measurements. It is observed that the normalized mean bias (NMB) is decreased by 39% and the fitted linear ratio between radar and rain gauge observation reaches at 0.98. Furthermore, the radar-based I-D threshold derived by the Frequentist method is $I = 10.1D^{-0.52}$, and it's also found that the I-D threshold is underestimated by uncorrected raw radar data. In order to verify the impacts on observations due to spatial variation, I-D thresholds are identified from the nearest rain gauge observations and radar observations at the rain gauge locations. It is found that both kinds of observations have similar I-D threshold and likewise underestimate I-D thresholds owing to under shooting at the core of convective rainfall. It is indicated that improvement of spatial resolution and measuring accuracy of radar observation will lead to the improvement of identifying debris flow occurrence, especially for events triggered by the small-scale strong rainfall process in the study area.

1 Introduction

Rainfall-induced debris flow is a kind of ubiquitous natural hazard for the mountain area with complex terrain. It is a geomorphic movement process which scour the sediment from steep areas into alluvial fans. The formation of rainfall-induced debris flow is generally related to three main factors, including the gravitational potential energy, abundant loose materials and meteorological events (Guzzetti et al., 2008). The gravitational potential energy relatively remains stable for a long period of time. The loose materials are normally made up of sand, unsorted silt, cobbles, gravel, boulders and woody debris (Wang et al., 2016). High magnitude level earthquake events can generate abundant loose solid material from co-seismic rock falls and landslides, and deposited in gullies (Shieh et al., 2009). During the rainy season, the occurrence of Debris flow after an earthquake becomes more frequent (Yu et al., 2014; Guo et al., 2016a). Both the Ms 8.0 Wenchuan earthquake on May 12, 2008 and the Ms 7.0 Lushan earthquake on April 20, 2013 occurred in Sichuan province of China and have changed the formation conditions for debris flow. A large number of debris flow occurred from 2008 to 2014 and caused lots of casualties and extensive property damage.

Early Warning System (EWS) for rainfall-induced landslide and debris flow are widely implemented in many parts of the world(Baum and Godt, 2010; Glade and Nadim, 2014; Segoni et al., 2015).The performance of EWS highly relies on the updating of precipitation thresholds (Rosi et al., 2015). Furthermore, considering the material condition of forming debris flow is vastly changed at earthquake affected region (Tang et al., 2009; Tang et al., 2012), it is necessary to revaluate the precipitation threshold. The model of rainfall Intensity-Duration is widely used to represent the precipitation thresholds of triggering landslides and debris flow (Aleotti, 2004; Guzzetti et al., 2007). Some literatures concluded that the I–D relationships for some of the regions were severely affected by the Wenchuan Earthquake (Su et al., 2012; Cui et al., 2013; Zhou and Tang, 2014; Guo et al., 2016b). However, most of these I-D relationships are derived from rain gauge observation. This is a common technical way to estimate the I-D thresholds of debris flows using rainfall observation from the nearest rain gauge. However, the uncertainty of intensity-duration thresholds from rain gauge observations could not be ignored. This is related to two critical limitations which probably lead to underestimation of observation of strong convective events occurring at high altitude area. The first limitation is the relatively sparse network density of rain gauges in the mountainous region (Marra et al., 2014), the other one is the altitude of gauge deployments which is at low elevation for sustainability. The same limitations of rain gauge observation also exist in the mountainous regions of Sichuan province. The technique of microwave remote sensing has become a necessary way for observing rainfall events in complex terrain. The radar-based quantitative precipitation estimation (QPE) has been demonstrated useful for the study of debris flows, as its unique advantage of high spatial and temporal resolution. Radar observation offer the unique merit of estimating rainfall over the actual debris flow location (David-Novak et al., 2004; Chiang and Chang, 2009; Marra et al., 2014; Berenguer et al., 2015). However, there are many challenges when Radar-based QPE in the mountainous area is applied in the study of debris flow. Commonly, keeping the elevation angle close to the ground and estimating the sample cut at the same height is a basic requirement for radar QPE to represent the actual rainfall distribution on the ground. The radar beam blocked by the mountain is a serious problem for the low angle observation.

The radar beam angle has to be elevated to avoid the blockage. However, doing this introduces another problem which is rainfall distribution at higher heights is different from that of at the surface and it also varies largely according to the precipitation type (Zhang et al., 2012). Errors due to radar system calibration and uncertainty in hydrometeor's DSD (Drop Size Distribution) also decrease the accuracy of rainfall estimates. Therefore, the combination of using radar and rain gauges to provide accurate rainfall estimates in complex terrain attracts increasingly more interest for improving warnings of future precipitation and situational awareness(Willie et al., 2017). Furthermore, debris flow triggering events are often related to high precipitation gradients of storms which occur for a short duration and have small scale (Nikolopoulos et al., 2015). Considering these, raw S-band radar reflectivity data are used to estimate rainfall, and assess the impact of estimation errors on the identification of I-D threshold over the study area.

The main aim of this study is to merge the radar QPE, thereby improving its estimation over complex terrain and to assess the impact of rainfall estimate accuracy on the identification of I-D threshold over the study area. To do that, a series of accuracy-improving measures have been adopted including a hybrid scan mode, the vertical reflectivity profile (VPR) correction, the mosaic of reflectivity, a combination of rainfall-reflectivity(R-Z) relationship for convective and stratiform rainfall and rainfall bias adjustment with Kalman filter (KF). Three radar rainfall estimation scenarios are evaluated with the rain gauge observations for six debris-flow triggering rainfall event to validate the accuracy of radar estimate. I-D thresholds are identified from 519 rainfall-induced debris flow events with the frequentist method (Brunetti et al., 2010; Peruccacci et al., 2012). Another aim of this study is to understand the impact on the I-D identification due to spatial variability of rainfall observation. Rain gauge observations nearest to the debris flow within 10 km and radar observations at the rain gauge locations are used to get the I-D relationship.

2. Study domain and data

The study area is located at Sichuan Province in southwest China which consists of 16 administrative districts and counties. The area of study is about 38,000 km^2 and occupies nearly 8% of the land area of Sichuan Province (see Figure 1). This area was strongly affected by the Ms8.0 Wenchuan earthquake which occurred in 12th May, 2008 and the Ms7.0 Lushan earthquake which occurred in 20th April, 2013. In the following years, debris flow happened frequently. During the period from 2012 to 2014, the debris flow occurring in this area accounted for 58.3% of the annual debris flows events which occurred in the whole province. The area is in the transitional zone of the Qinghai-Tibet Plateau to the Sichuan Basin. Terrain changes steeply and the average altitude above sea level (a.s.l) for this area is between 500 meters and 6 kilometres. The geological structure of the study area show a northeast to southwest orientation. The rocks over this region are mainly comprised of volcanic rocks, mixed sedimentary rocks, siliciclastic sedimentary rocks, carbonate sedimentary rocks, acid plutonic rocks, intermediate colcanic rocks, intermediate plutonic rocks, unconsolidated sediments, metamorphic rocks, basic Plutonic Rocks, and pyroclastic rocks. Figure 1a shows the lithological map. Quaternary deposits were distributed in the form of river terraces and alluvial fans.

Owing to frequent tectonic activities, most of the gully are steeply sloped over this area, as shown in the Figure 2a. The main land use types in this region are mixed forest, cropland, and grassland, as shown in Figure 2b.Potential DF watersheds over study area were extracted from morphological variables, using the logistic regression method. M. Berenguer(2015) simplified the geomorphological variables, as the watersheds maximum height (h_{max}), mean slope (s_{mean}), mean aspect (θ_{mean}) and melton ratio (MR) are the variables with the smallest overlapping areas for assessing the susceptibility of the watersheds. The h_{max}, s_{mean}, θ_{mean} and MR were retrieved from DEM data. Combined with the DF occurrence over this area during the three years, the potential susceptibility map was calculated with logarithm regression method, as shown in the figure 3. The identification results show that there are 673 potential debris flow watersheds in this region.

The climate type of the study area is humid subtropical. The monthly precipitation distribution is commonly affected by the plateau monsoon, the East Asian monsoon and complex terrain. The mean annual rainfall over the central and southern parts of this region varies from 1200 to 1800 mm, and sometimes even reaches 2500 mm (Xie et al., 2009).The mean annual rainfall over the western part of this area is less than 800 mm. The north and southwestern areas of this region are in the transition zone from hot dry to humid climates, with mean annual precipitation ranging between 800 and 1200 mm.

The area is monitored by two well-maintained S-band Doppler weather radars (see Figure 1). One is deployed in Chengdu city with an altitude of 596m above the sea level and the other one is deployed at Mianyang city with the height of 557m above the sea level. Both of the radar systems have same system specifications which can be seen in table 1. The system provides radar rainfall estimates at a radial range resolution of 300 m and an angular resolution of 1 degree. There is a rain gauge network consisting of 551 gauges equipped at the meteorological surface station in the study areas. The number of rain gauges seems to be a lot, but most of them are deployed at the valleys. The density of rain gauges is severely scarce at the high altitude of the mountain, resulting in observation gaps where the debris flow initially takes place. The average altitude above sea level of those rain gauges is far lower than 3km.

3. Methods

3.1 Radar accumulated rainfall estimation methods

S-band weather radar has a unique advantage of being unaffected by attenuation, as it is subjected to Rayleigh scattering for almost all hydrometeors. However, in complex terrain conditions, S-band radar observations still face serious challenges. The main problem comes from ground clutter and severe beam blockage, resulting in inaccurate estimates of radar rainfall. A number of signal processing techniques have been developed to detect and remove clutter and anomalous propagation (AP), including fuzzy logic, ground echo maps, Gaussian Model adaptive processing (GMAP) filter, etc. (Harrison et al., 2000; Berenguer et al., 2006; Nguyen and Chandrasekar, 2013). For the radar data used in this study, ground clutter is filtered with the GMAP algorithm configured in Vaisala Sigmet digital processor. Furthermore, in order to overcome the beam blockage and improve the rainfall estimation accuracy, radar data are corrected concerning the following issues: (i) Beam shielding and

hybrid scan, (ii) Vertical profile of reflectivity, (iii) Mosaic of hybrid scan reflectivity, (iv) Combination of reflectivity rainfall relationship, (v) Rainfall bias adjustment.

Beam shielding and hybrid scan. The mode of Hybrid scan is used to form the initial reflectivity field for rainfall estimate, by keeping the radar main beam away from the blockage of the complex terrain(Zhang et al., 2012). In the study area, the grids with 0.36 km^2 resolution on the ground are aligned with radar bins of each elevation angle. The blockage coefficients of the low elevation angles at 0.5°, 1.5° and 2.4° are calculated according to the Digital Elevation Model(DEM), earth curvature, antenna pattern and the wave propagation model (Pellarin et al., 2002; Krajewski et al., 2006). The blockage ratio distribution of two S-band radar can be seen from figure 4. There are almost no topographical shielding in the near field within the distance of 50 km from each radar. The main factor considered in the hybrid scan within 50 km is to meet the estimated rainfall from the same vertical height as much as possible. Thus the area within 20 km from radar is assigned with the elevation angle of 3.4°, the area from radar between 20 and 35 km is assigned with the elevation angle of 2.4°, the area from radar between 35 and 50 km is assigned with the elevation angle of 1.5°. It is assigned with the elevation angle of 0.5° by default, if there is no blockage over 50km distance from the radar. The terrain transforms from plain land to mountainous region over about 70 km westward away from each radar. At this region the altitude rises sharply, and elevation angle of 0.5° is totally obscured. Therefore, the lowest angle at which the blockage ratio does not surpass 0.5 is assigned to the aligned grid. Meanwhile, the blockage ratio is correspondingly used to compensate the energy loss of reflectivity. The final adaptive-terrain hybrid scan maps are combined as shown in figure 4 (d) and (h). It can be seen that most of the study area are covered by the 1.5° and 2.4° of radar scan.

Vertical Profile of Reflectivity (VPR). Due to the hybrid scan, the radar elevation angle is raised resulting in majority of the observed reflectivity coming from the upper levels of precipitation profiles. This is quite different from the actual reflectivity on the ground. It is necessary to account for the reflectivity correction at the ground level. This study adopts the AVPR method to adjust the reflectivity (Zhang et al., 2012). The processing steps applied in this study include: (i) To discriminate convection precipitation from stratiform based on the composite reflectivity>50dBz or VIL >6.5 kg/m^2, where VIL is acronym of Vertically Integrated Liquid water content and it is an estimate of the total mass of precipitation in the clouds (Amburn and Wolf, 1997). (ii) The parameterization of VPR is carried out to generate bright band top, peak, bottom heights and piecewise linear slope S_1, S_2, and S_3(see Figure 5). (iii) Reflectivity observed is adjusted based on the parameterized VPR to piecewise extrapolate the corresponding reflectivity at the ground. Figure 5 shows a sample scatter plot of the vertical reflectivity profiles from 11: 30 to 12: 30 on July 21, 2012. Impacted by the temperature, air dynamic, particle size and phase are changed along the vertical falling. Figure 5 shows vertical profile of reflectivity varied approximately as three piecewise linear sections. Considering altitude is one the critical factor affecting the atmosphere physics parameters and the performance of VPR. The areas of study are classified as two types: region type I and II with the condition of the height from the ground (≤1.5 km for region type I and >1.5 km for region type II) and the distance from the radar (≤100 km for region type I and >100 km for region type II). Figure 6 shows

the identification result for both radars. Apart from the VPR adjustment, these two kinds of regions are respectively assessed during the validation of radar QPE, in order to understand the actual impact of distance and height of radar observations on the rainfall estimation.

Mosaic of hybrid scan reflectivity. Both of two S-band radar have common coverage areas where reflectivities data should be mosaicked to construct a large-scale sensing for rainfall events. Taking the distance and altitude as weighing parameters, the mosaic formula is define below:

$$Z_M = \frac{\sum_i w_i \times k_i \times Z_i}{\sum_i w_i \times k_i} \quad (1)$$

and

$$w_i = exp\left(-\frac{d_i^2}{L^2}\right) \quad (2)$$

$$k_i = exp\left(-\frac{h_i^2}{H^2}\right) \quad (3)$$

Here, Z_M represents the mosaicked hybrid scan reflectivity, Z_i is the single radar hybrid scan reflectvity, i is the radar index, w is weighing component for the horizontal weighting, and k is weighing component for the vertical weighting. The variable d is the distance between the analysis grid and the radar, and h is the height above the ground of the single radar hybrid scan. The parameters L and H are respectively scale factors of the two weighting functions.

Combination of rainfall relationship, Rainfall rates are calculated from radar reflectivity by a power law empirical relationship which is called *Z–R* relationship (Austin, 1987; Rosenfeld et al., 1993), and theoretically, the Z–R relationships should be adjusted when the drop size distributions (DSD) change over the rainfall duration. However, it is still a challenge to obtain fine spatial distribution of DSD with change of time over complex terrains. This study adopts the two widely verified Z-R relationships defined as: $Z = 300R^{1.4}$ for convective precipitation (Fulton et al., 1998) and $Z = 200R^{1.6}$ for stratiform (Marshall et al., 1955), and the rainfall type is identified during VPR processing.

Rainfall bias adjustment. The errors of R-Z relationship mainly come from raindrop size distribution (DSD) variation, radar calibration errors etc. (Berne and Krajewski, 2013), so the rainfall bias change over time. The mean field bias correction is a method to calculate the ratio of the means of radar estimate and the rain gauge observation (Anagnostou and Krajewski, 1999; Chumchean et al., 2003; Yoo and Yoon, 2010). In this study, the bias is calculated based on hourly radar rainfall accumulation and rain gauge accumulated observation. It's defined as:

$$BIAS = \frac{\frac{1}{N}\sum_i^N r_i}{\frac{1}{N}\sum_i^N g_i} \quad (4)$$

where $BIAS$ is mean rainfall bias in one hour, g is one hour accumulated rainfall of rain gauge, i is rain gauge index, r is the radar-based one hour accumulated rainfall over the i-th rain gaugee and N is the total number of rain gauges. As described above, the density of rain gauge deployment over the mountainous area is relatively scarce. Therefore the precipitation measured by individual gauges at high and low altitudes may lead to overestimation and underestimation respectively. Therefore, the Kalman filter is adopted to alleviate the measurements noise of the bias (Ahnert, 1986; Chumchean et al., 2006; Kim and Yoo, 2014).

The basic steps of Kalman filter in this study include:

Step 1 State estimate prediction:

$$BIAS_P(n) = BIAS_{KF}(n-1) \quad (5)$$

where:$BIAS_P$ represents the bias prediction, $BIAS_{KF}$ represents the bias estimate update, n is discrete time.

Step 2 State estimate error covariance prediction:

$$P_P(n) = F^2 \times P_{KF}(n-1) + Q \quad (6)$$

where: P_P represents the bias estimate error covariance prediction. P_{KF} represents the bias estimate error covariance update. Q represents covariance function of the system error.

Step 3 Calculating Kalman gain

$$G(n) = P_P(n) \times \left(P_P(n) + S\right)^{-1} \quad (7)$$

where: G represents the Kalman gain. S represents covariance function of the measurement error.

Step 4 Updating State estimate

$$BIAS_{KF}(n) = BIAS_P(n) + G(n) \times \left[BIAS_m(n) - BIAS_P(n)\right] \quad (8)$$

where:$BIAS_m$ represents the bias measurement.

Step 5 Updating estimate error covariance

$$P_{KF}(n) = \left(1 - G(n)\right) \times P_P(n) \quad (9)$$

It is assumed that the variation of the real bias within each hour is negligible, the initial estimator for mean field radar rainfall logarithmic bias and its error variance are assumed to equal their update values which are respectively the $BIAS_{KF}(0)$ and $P_{KF}(0)$.

3.2 Intensity-Duration threshold identification methods

Rainfall thresholds for the possible initiation of debris flows are identified according to the I–D power law relationship (Guzzetti et al., 2007). , it's defined as bellows:

$$I = \alpha D^{-\beta} \quad (10)$$

Calculating the event duration (D) and the average intensity (I) requires the start and end times of the rainfall event. The duration and intensity of each debris flow can be directly identified with the time-sequential radar rainfall estimate .These times are determined by an interval of at least 24 hours, rain rates of less than 0.1 mm h^{-1} (Guzzetti et al., 2008; Marra et

al., 2014), or correspondingly radar reflectivity of less than 10 dBz to separate two consecutive rainfall events. The parameters of a and β are estimated with the Frequentist method (Brunetti et al., 2010).

In order to illustrate the impacts of radar rainfall estimate on I-D threshold, basic procedures of the frequentist method are applied to radar rainfall accumulation and are described below:

(i) Radar-identified rainfall durations and average intensities are log transformed as $\log(I)$, $\log(D)$. Both of them are fitted by least square method to form a linear equation as $\log(I_f) = \log(\alpha_{50}) - \beta\log(D)$, where α_{50} , β is the fitted intercept and slope, respectively .

(ii) For each debris flow, the difference $\delta(D)$ between the actual rainfall average intensity $\log[I(D)]$ and the corresponding fitted intensity value $\log[I_f(D)]$ is calculated, $\delta(D) = \log[I(D)] - \log[I_f(D)]$.

(iii) The probability density function (PDF) of the of $\delta(D)$ distribution is determined through Kernel Density Estimation and furthermore fitted with a Gaussian function, which is defined as:

$$f(\delta) = a \times exp\left(-\frac{(\delta - b)^2}{2c^2}\right) \quad (11)$$

where a>0, c >0, and $a, b, c \in \mathbb{R}$.

(iv) The threshold for expected minimum exceedance probability (P_{mep}) is determined by PDF function, as

$$\int_{-\infty}^{\delta_{mep}} f(\delta)\, d\delta = P_{mep} \quad (12)$$

where δ_{mep} is the intercept parameters. δ_{mep} can be resolved through Equ.(12) for given P_{mep}, then the α_{mep} corresponding to the P_{mep} is calculated as

$$\alpha_{mep} = \alpha_{50} exp(\delta_{mep}) \quad (13)$$

Finally, α_{mop} and β are best fitted parameters for exceedance probabilities P_{mep}.

The minimum exceedance probability is set to 5% for this study.

4. Events, result and discussion

Six debris-flow triggering rainfall events which occurred in the area of study between 2012 and 2014 are analysed. Those events happened at the most severe earthquake affected region during rainy season and triggered a total of 519 debris flow that caused casualties and extensive property damage. Table 2 summarizes the characteristics of the rainfall events. Three events occurred in August, two events occurred in July and one occurred in June. These events are deemed to be representative of the debris flow-triggering precipitation in the region during the rainy season. The event duration time and maximum rainfall accumulation are also retrieved by the rain gauge nearest to debris flow location and radar observations. The identification of rainfall event was determined by an interval of at least 24 hours, the rain rate is less than 0.1 mm/h (Guzzetti et al., 2008; Marra et al., 2014). Table 2 indicates that the durations and rainfall accumulations identified by gauge and radar are different owing

to the precipitation type and density of rain gauges. The identification differences of event No.1, 2, and 6 between gauge and radar are not so large like event No. 3, 4, and 5. From the figure 7 of radar-estimated rainfall accumulation for the six rainfall events (the improving measures described below are applied in the figure 7), it can be seen that the precipitation of event No.3, 4 and 5 is dominated by convective and the strong core of rainfall region is located at the high altitude area where rain gauge is relatively scarce. A few of debris flow occurred at the long range, approaching radar detection edges, while the rainfall measured there was low. This may be caused by the decreasing resolution at long radial range. In following section, rainfall estimation accuracy, I-Dthe distance and height are considered as an evaluation factor to assess the radar-based rainfall estimate. Considering the accuracy and robustness of the I-D threshold of the debris flow are determined by the accuracy of rainfall observation and positioning, a series of processing including hybrid scan, VPR correction, a combined R-Z relationship, and mean bias adjustment is performed on six rainfall event to improve the accuracy of radar-based accumulated rainfall. In order to evaluate the overall performance and verify the impact on I-D threshold due to rainfall accumulation accuracy, the assessment was performed towards three scenarios of radar-based estimates: scenario I, the estimate from raw data of hybrid scan without VPR and bias adjustment; scenario II, the estimates with VPR adjustment after scenario I; scenario III, the estimates with rainfall bias correction after scenario II. According to rainfall estimate evaluation, I-D thresholds are derived from those scenarios and also assessed concerning accuracy and spatial resolution.

4.1Assessment of rainfall estimation accuracy

The accuracy of the radar-based event rainfall accumulation is assessed with the rain gauge observation. In order to perform evaluation, a set of criterions is calculated including normalized standard error (NSE), normalized mean bias (NMB) and correlation coefficient (CORR), defined as below:

$$NSE = \frac{\frac{1}{N}\sum_i^N |r_i - g_i|}{\frac{1}{N}\sum_i^N g_i} \times 100\% \quad (14)$$

$$NMB = \frac{\frac{1}{N}\sum_i^N (r_i - g_i)}{\frac{1}{N}\sum_i^N g_i} \times 100\% \quad (15)$$

$$CORR = \frac{\sum_i^N (g_i - \bar{g})(r_i - \bar{r})}{\sqrt{\sum_i^N (g_i - \bar{g})^2}\sqrt{\sum_i^N (r_i - \bar{r})^2}} \quad (16)$$

where NMB and NSE are in percent, CORR is dimensionless, r_i and g_i represent the rainfall accumulation from radar and gauge, N is the total sampling number. The statistical criterions comparisons between radar-rain gauge and the three radar estimate scenarios are shown in table 3, and the scatter plot of radar-based estimates and rain gauge rainfall observations are shown in figure 8. The comparison for scenario I indicates: The NSE, NMB and CORR of the whole study areas are 50.7%, -41.1% and 0.78 respectively. The radar-based rainfall is underestimated. The linear ratio is estimated from linear regression

of radar rainfall estimation and rain gauge observation, with the predefined intercept of zero. The linear ratio approximates to one, if radar-based rainfall estimation is consistent with rain gauge observation. The linear ratio of rainfall observation between radar and gauge for scenario I is 0.51, as shown in figure 8(a). The reason of underestimation is the systematic bias and uncertainty of reflectivity on the ground. From the comparison of two type regions, it can be observed, the NSE, NMB and CORR of region type I are relatively better than region type II. It is revealed that improving measure are needed for the hybrid scan estimate.

The comparison for scenario II indicates: The NSE, NMB and CORR for the study areas are 46.1%, -18.6% and 0.80 respectively. It is an improvement compared with the scenario I. The radar-based rainfall is also underestimated through the VPT adjustment, and the linear ratio of rainfall observation between radar and gauge is 0.76, as shown in figure 8(b). This means rainfall biases still exist in the estimate. The NSE and CORR of region type I are also slightly better than region type II.

The comparison for scenario III indicates: The NSE, NMB and CORR of the whole study areas are 44.0%, 1.91% and 0.84 respectively. The linear ratio of rainfall observation between radar and gauge is 0.98, as shown in figure 8(c), and this means the consistency between rainfall and radar observation is achieved through the Kalman filter-based bias correction. Figure 9 shows the average and covariance of bias estimation by Kalman filter and mean field bias method for six rainfall event. The CORR and NSE improvement also verify the efficiency of Kalman-filter for radar QPE in mountainous areas, Kalman filtering makes the whole rainfall event estimate free from large significant overestimation or underestimation.

Scenario III provides the optimum rainfall estimation for this study. In the following, all of the three scenarios are used to assess the impact of QPE accuracy on I-D relationship identification.

4.2 Intensity-duration thresholds based on radar QPE

The radar rainfall estimates with high spatial resolution can retrieve rainfall duration and average intensity for each rainfall-triggered debris flow, so an abundant of sample data are captured to induce the I-D relationship. Scatter distribution of event duration-intensity for the three radar estimated scenarios are shown in figure 10, Comparisons of scatter distribution between each other's indicate that the average rainfall intensity and duration are incrementally increased when applying the improving measures. The PDF estimations reveal that the number of positive difference $\delta(D)$ is more than the number of negative difference. This can be accounted for storm triggering which is relatively dominant. The parameters of Gaussian function are summarized in table 4. The parameter a is incrementally decreasing. When applying the improving measures, parameter c has the opposite changing trend and parameter b is randomly changes around the small range of zero.

The I-D threshold derived from the scenario III is $I = 10.1D^{-0.52}$. It is higher than the other two I-D thresholds derived from scenario I and scenario II, owing to application of accuracy improving measuring.

4.3 comparison with intensity–duration thresholds from rain gauge observations

In order to analyze the impact of the spatial sampling variability on identification of I-D threshold for radar estimate and rain gauge observation, I-D threshold are derived from rain gauge nearest to the debris flow and radar estimate at the corresponding the co-location of rain gauge(Marra et al., 2014). There are some same predefined conditions for comparison: (1) duration times are identified separately by two kinds of sensors, rainfall duration time is required to be more than 1 hour and minimum mean rainfall rate is 0.1 mm/h. (2) the maximum distance from debris flow location is less than 10km.(3) identification of I-D threshold calculated from frequentist methods with exceedance probabilities of 0.5%.Firstly, the event rainfall accumulation are compared between rain gauge observations nearest to the location of debris flows and radar estimates at the location of the corresponding rain gauge. The scatter plot of rain gauge and radar estimate is shown in figure 11. The corresponding metrics are calculated. The CORR is 0.88, NMB is 17.07%, NSE is 28.32% and linear ratio is 1.13, indicating that rainfall observations from rain gauge nearest to debris flows location and radar estimate at co-location have the tendency of consistency. The I-D threshold are derived from rain gauge and radar estimate. Scatter plots of I-D pairs are shown in Figure 12,The I-D threshold estimated from rain gauge is $I = 5.1D^{-0.42}$, The other I-D threshold estimated from radar is $I = 5.8D^{-0.41}$.Both of I-D thresholds seem little lower than $I = 10.1D^{-0.52}$, since the scarce gauge network didn't capture the strong core of rainfall which triggered the debris flow. It is interesting to note that both I-D thresholds of radar and rain gauge are very similar, although there are some measurement errors between them as shown in figure 11.

4.4 Impact of rainfall spatial variation on Intensity and Duration

The accumulated rainfall, duration and rainfall intensity identified from the nearest rain gauge probably are different from the realities occurred at the debris flow location, since the rainfall varies in space especially for convective precipitation with sharp variation in short distance. The observed rainfall differences rely on the distance from the nearest rain gauge to the debris location and could be considered as spatial errors. To this end, relative errors of the accumulated rainfall, duration, and rainfall intensity versus distance are calculated from the comparisons with the radar-based estimate at the location of debris flow. The metrics for evaluating relative error versus distance are defined in table 5. There are also some predefined conditions for the comparison of relative errors versus distance: (1) The radar rainfall estimation used for comparison are all from scenario III. (2) The radar rainfall estimation and duration identification at the debris flow location are considered as the true referred value. (3) The maximum distance from debris flow location to the nearest rain gauge is predefined within 10 km and the distance resolution is set equal to those two CINRADs' range resolution of 300 meters. (4) In order to assess the rainfall spatial variation using multi-sensor, the radar-based estimate at the co-location of the nearest rain gauge, as well as rain gauge observation, is also compared with the radar-based estimate at the location of debris flow.

The metrics of Accumulated Rainfall Relative Error (ARRE), Duration Relative Error (DRE) and Rainfall Intensity Relative Error (RIRE) are calculated for the nearest rain gauge and radar estimate at the co-location respectively. The results of ARRE,

DRE and RIRE versus distance are drawn in Figure 13. The main findings from the evaluation results are summarized as follows:

(1) The results of ARRE, DRE and RIRE all have an enlarging tendency along with the increasing distance. The maximum ARRE, DRE and RIRE for rain gauge observation is 42.2%, 41.67% and 55.88%, respectively. The maximum ARRE, DRE and RIRE for radar-based estimate at the co-location of the nearest rain gauge is 43.33%, 41% and 45.2%, respectively.

(2) Nonlinear regression is applied for ARRE, DRE and RIRE versus distance to investigate the average tendency, as shown in the figure 13. The regression curves of ARRE and DRE for rain gauge and radar are approximately similar within 10km and 4km, respectively, indicating radar estimate and rain gauge observation have the similar rainfall spatial variation impacts.

It is clarified from the above discussion that the rainfall estimation accuracy and spatial variation impact the identification of I-D threshold. We further take the α and β estimated from Scenario III as a right referred value, and calculate the relative error of α and β for each scenario, as shown in the table 6. The relative error of α for Scenario I, II, and III is -24.5%, -13.8% and 0%, respectively. The relative error of β for Scenario I, II, and III is -28.8%, -17.3% and 0%, respectively. It is indicated that improving the accuracy of rainfall estimate is able to decrease the relative errors of α and β, Concerning rainfall spatial variation, the relative error of α for the nearest gauge observation and radar-based estimate at the co-location is -49.5% and -42.6%, respectively. The relative error of β for the nearest gauge observation and radar-based estimate at the co-location is -19.5% and -21.2%, respectively. The relative error of α is remarkably larger than the one derived from radar-based estimate on the debris flow location, however, the differences of α and β for rain gauges and radar-based estimate at the co-location are not significant.

4.5 Comparison with previous results

The I–D threshold for the study regions is compared with other global, regional thresholds in the literature. It can be seen from figure 14 that the thresholds obtained in this work (red in Figure 14) fall in the range of other I-D thresholds. The results were also compared with the rainfall thresholds previously proposed in the Wenchuan Earthquake area (Tang et al., 2012; Zhou and Tang, 2014; Guo et al., 2016a). Our result lies at the middle range of them. The difference comes from the database we used, the radar data which is used to fill the observation gap of rain gauges, and the identification method of I-D threshold were also different due to a different exceedance probability. The I–D threshold of this study is crossed checked with that proposed in the Chi-chi Earthquake affected area in Taiwan (Chien Yuan et al., 2005), mainly owing to the climatic differences like storm occurrence duration and intensity. The result nearly overlapped with the one proposed in Adige area of Italy (Marra et al., 2014). The I-D threshold is lower than the cases for Japan (Jibson, 1989) and for the world (Caine, 1980), but higher than the world (Guzzetti et al., 2008).

Summary

The main purpose of this paper is to evaluate the debris flow occurrence thresholds of the rainfall intensity-duration in the earthquake-affected areas of Sichuan province over the rainy seasons from 2012 to 2014. The paper calculates the Intensity-Duration threshold from radar-based rainfall estimate, which is different from the common method of using rain gauge observation. Radar observations have high spatial resolutions sensitive to convective precipitation, which is a critical issue for rain gauge observation owing to its scarcity and low altitude deployment over mountain areas. However, the accuracy of radar-based QPE over complex areas is affected by the terrain and remains a challenge for hydrological application. The following works were done to draw the conclusions.

(a) There are two S-band Doppler radars covering the study area. Radar observations for six rainfall events were processed with a series of mountain-oriented QPE algorithms including: a terrain-adapted hybrid scan, VPR correction, the reflectivity mosaic, the combination of R-Z relationships, and rainfall bias correction. Three types of estimation from radar are performed and compared with rain gauge observations to validate the accuracy. The results show that: The combination of the whole correction procedures reduces the bias to 1.91% and the NSE to 44%, meanwhile improves the correlation coefficient to 0.84 and the linear ratio to 0.98.

(b) Intensity Duration rainfall thresholds for the triggering debris flow are calculated with a frequentist approach. The I-D threshold of $I = 10.1D^{-0.52}$ is derived from the kalman filter corrected radar estimates. The accumulated rainfall is lower than rain gauge observations and the derived I-D is also underestimated. The hybrid scan, VPR correction and combination of R-Z relationship are strongly required.

(c) The I-D deduced from rain gauge observations nearest to the occurrence of debris flow is highly similar to the one deduced from the radar estimates at the same location as rain gauge, which are $I = 5.1D^{-0.42}$ and $I = 5.8D^{-0.41}$ respectively. These I-D thresholds are underestimated owing to the rainfall spatial variation and the incontinuous sampling effect.

Finally, it is clear that radar-based rainfall estimate and threshold supplement the monitoring gap of EWS where rain gauge is scarce. A better understanding of relationship between rainfall and debris flow initiation for earthquake affected area can be enhanced by improving the spatiotemporal resolution and low elevation angle coverage of radar observation, especially for monitoring the convective storm occurring at the mountains.

Acknowledgements. This research was supported by the National Natural Science Foundation of China (No. 41505031), China Scholarship Council (No.201508515021), the Science and Technology Support Project of Sichuan Province (No. 2015SZ0214), Scientific Research Funding of CUIT (No. J201603), China Meteorological Bureau Meteorological Sounding Engineering Technology Research Centre Funding. We appreciate the weather bureau of Sichuan Province for the data services.

References

Ahnert, P.: Kalman filter estimation of radar-rainfall field bias, Preprints of the 23rd Conference on Radar Meteorology, 1986,

Aleotti, P.: A warning system for rainfall-induced shallow failures, Engineering Geology, 73, 247-265, 10.1016/j.enggeo.2004.01.007, 2004.

Amburn, S. A., and Wolf, P. L.: VIL density as a hail indicator, Weather and forecasting, 12, 473-478, 1997.

Anagnostou, E. N., and Krajewski, W. F.: Real-time radar rainfall estimation. Part I: Algorithm formulation, Journal of Atmospheric and Oceanic Technology, 16, 189-197, 1999.

Austin, P. M.: Relation between measured radar reflectivity and surface rainfall, Monthly Weather Review, 115, 1053-1070, 1987.

Baum, R. L., and Godt, J. W.: Early warning of rainfall-induced shallow landslides and debris flows in the USA, Landslides, 7, 259-272, 2010.

Berenguer, M., Sempere-Torres, D., Corral, C., and Sánchez-Diezma, R.: A fuzzy logic technique for identifying nonprecipitating echoes in radar scans, Journal of Atmospheric and Oceanic Technology, 23, 1157-1180, 2006.

Berenguer, M., Sempere-Torres, D., and Hürlimann, M.: Debris-flow forecasting at regional scale by combining susceptibility mapping and radar rainfall, Natural Hazards and Earth System Science, 15, 587-602, 10.5194/nhess-15-587-2015, 2015.

Berne, A., and Krajewski, W. F.: Radar for hydrology: Unfulfilled promise or unrecognized potential?, Advances in Water Resources, 51, 357-366, 10.1016/j.advwatres.2012.05.005, 2013.

Brunetti, M., Peruccacci, S., Rossi, M., Luciani, S., Valigi, D., and Guzzetti, F.: Rainfall thresholds for the possible occurrence of landslides in Italy, Natural Hazards and Earth System Sciences, 10, 447-458, 2010.

Caine, N.: The rainfall intensity: duration control of shallow landslides and debris flows, Geografiska Annaler. Series A. Physical Geography, 23-27, 1980.

Chiang, S.-H., and Chang, K.-T.: Application of radar data to modeling rainfall-induced landslides, Geomorphology, 103, 299-309, 10.1016/j.geomorph.2008.06.012, 2009.

Chien Yuan, C., Tien-Chien, C., Fan-Chieh, Y., Wen-Hui, Y., and Chun-Chieh, T.: Rainfall duration and debris-flow initiated studies for real-time monitoring, Environmental Geology, 47, 715-724, 2005.

Chumchean, S., Sharma, A., and Seed, A.: Radar rainfall error variance and its impact on radar rainfall calibration, Physics and Chemistry of the Earth, Parts A/B/C, 28, 27-39, 2003.

Chumchean, S., Seed, A., and Sharma, A.: Correcting of real-time radar rainfall bias using a Kalman filtering approach, Journal of Hydrology, 317, 123-137, 2006.

Cui, P., Zou, Q., Xiang, L.-z., and Zeng, C.: Risk assessment of simultaneous debris flows in mountain townships, Progress in physical geography, 37, 516-542, 2013.

David-Novak, H. B., Morin, E., and Enzel, Y.: Modern extreme storms and the rainfall thresholds for initiating debris flows on the hyperarid western escarpment of the Dead Sea, Israel, Geological Society of America Bulletin, 116, 718-728, 2004.

Fulton, R. A., Breidenbach, J. P., Seo, D.-J., Miller, D. A., and O'Bannon, T.: The WSR-88D rainfall algorithm, Weather and Forecasting, 13, 377-395, 1998.

Guo, X., Cui, P., Li, Y., Ma, L., Ge, Y., and Mahoney, W. B.: Intensity–duration threshold of rainfall-triggered debris flows in the Wenchuan earthquake affected area, China, Geomorphology, 253, 208-216, 2016a.

Guo, X., Cui, P., Li, Y., Zou, Q., and Kong, Y.: The formation and development of debris flows in large watersheds after the 2008 Wenchuan Earthquake, Landslides, 13, 25-37, 2016b.

Guzzetti, F., Peruccacci, S., Rossi, M., and Stark, C. P.: Rainfall thresholds for the initiation of landslides in central and southern Europe, Meteorology and atmospheric physics, 98, 239-267, 2007.

Guzzetti, F., Peruccacci, S., Rossi, M., and Stark, C. P.: The rainfall intensity–duration control of shallow landslides and debris flows: an update, Landslides, 5, 3-17, 2008.

Harrison, D., Driscoll, S., and Kitchen, M.: Improving precipitation estimates from weather radar using quality control and correction techniques, Meteorological Applications, 7, 135-144, 2000.

Jibson, R. W.: Debris flows in southern Puerto Rico, Geological Society of America Special Papers, 236, 29-56, 1989.

Kim, J., and Yoo, C.: Use of a dual Kalman filter for real-time correction of mean field bias of radar rain rate, Journal of Hydrology, 519, 2785-2796, 10.1016/j.jhydrol.2014.09.072, 2014.

Krajewski, W. F., Ntelekos, A. A., and Goska, R.: A GIS-based methodology for the assessment of weather radar beam blockage in mountainous regions: two examples from the US NEXRAD network, Computers & geosciences, 32, 283-302, 2006.

Marra, F., Nikolopoulos, E. I., Creutin, J. D., and Borga, M.: Radar rainfall estimation for the identification of debris-flow occurrence thresholds, Journal of hydrology, 519, 1607-1619, 2014.

Marshall, J., Hitschfeld, W., and Gunn, K.: Advances in radar weather, Advances in geophysics, 2, 1-56, 1955.

Nguyen, C. M., and Chandrasekar, V.: Gaussian Model Adaptive Processing in Time Domain (GMAP-TD) for Weather Radars, Journal of Atmospheric and Oceanic Technology, 30, 2571-2584, 10.1175/jtech-d-12-00215.1, 2013.

Nikolopoulos, E. I., Borga, M., Creutin, J. D., and Marra, F.: Estimation of debris flow triggering rainfall: Influence of rain gauge density and interpolation methods, Geomorphology, 243, 40-50, 10.1016/j.geomorph.2015.04.028, 2015.

Pellarin, T., Delrieu, G., Saulnier, G.-M., Andrieu, H., Vignal, B., and Creutin, J.-D.: Hydrologic visibility of weather radar systems operating in mountainous regions: Case study for the Ardeche catchment (France), Journal of Hydrometeorology, 3, 539-555, 2002.

Peruccacci, S., Brunetti, M. T., Luciani, S., Vennari, C., and Guzzetti, F.: Lithological and seasonal control on rainfall thresholds for the possible initiation of landslides in central Italy, Geomorphology, 139-140, 79-90, 10.1016/j.geomorph.2011.10.005, 2012.

Rosenfeld, D., Wolff, D. B., and Atlas, D.: General probability-matched relations between radar reflectivity and rain rate, Journal of applied meteorology, 32, 50-72, 1993.

Rosi, A., Lagomarsino, D., Rossi, G., Segoni, S., Battistini, A., and Casagli, N.: Updating EWS rainfall thresholds for the triggering of landslides, Natural Hazards, 78, 297-308, 2015.

Segoni, S., Battistini, A., Rossi, G., Rosi, A., Lagomarsino, D., Catani, F., Moretti, S., and Casagli, N.: An operational landslide early warning system at regional scale based on space–time-variable rainfall thresholds, Natural Hazards and Earth System Sciences, 15, 853-861, 2015.

Shieh, C.-L., Chen, Y., Tsai, Y., and Wu, J.: Variability in rainfall threshold for debris flow after the Chi-Chi earthquake in central Taiwan, China, International Journal of Sediment Research, 24, 177-188, 2009.

Su, P., Wei, F., and Cheng, Z.: Debris flow activity of Mozi Gully after Wenchuan earthquake on May 12, J Yangtze River Sci Res Inst, 29, 16-22, 2012.

Tang, C., Zhu, J., Li, W., and Liang, J.: Rainfall-triggered debris flows following the Wenchuan earthquake, Bulletin of Engineering Geology and the Environment, 68, 187-194, 2009.

Tang, C., van Asch, T. W., Chang, M., Chen, G., Zhao, X., and Huang, X.: Catastrophic debris flows on 13 August 2010 in the Qingping area, southwestern China: the combined effects of a strong earthquake and subsequent rainstorms, Geomorphology, 139, 559-576, 2012.

Wang, Q., Kong, Y., Zhang, W., Chen, J., Xu, P., Li, H., Xue, Y., Yuan, X., Zhan, J., and Zhu, Y.: Regional debris flow susceptibility analysis based on principal component analysis and self-organizing map: a case study in Southwest China, Arabian Journal of Geosciences, 9, 718, 2016.

Willie, D., Chen, H., Chandrasekar, V., Cifelli, R., Campbell, C., Reynolds, D., Matrosov, S., and Zhang, Y.: Evaluation of Multisensor Quantitative Precipitation Estimation in Russian River Basin, Journal of Hydrologic Engineering, 22, E5016002, 10.1061/(asce)he.1943-5584.0001422, 2017.

Xie, H., Zhong, D., Jiao, Z., and Zhang, J.: Debris flow in Wenchuan quake-hit area in 2008, Journal of Mountain Science, 27, 501-509, 2009.

Yoo, C., and Yoon, J.: A proposal of quality evaluation methodology for radar data, Journal of The Korean Society of Civil Engineers, 30, 2010.

Yu, B., Wu, Y., and Chu, S.: Preliminary study of the effect of earthquakes on the rainfall threshold of debris flows, Engineering Geology, 182, 130-135, 2014.

Zhang, J., Qi, Y., Kingsmill, D., and Howard, K.: Radar-Based Quantitative Precipitation Estimation for the Cool Season in Complex Terrain: Case Studies from the NOAA Hydrometeorology Testbed, Journal of Hydrometeorology, 13, 1836-1854, 10.1175/jhm-d-11-0145.1, 2012.

Zhou, W., and Tang, C.: Rainfall thresholds for debris flow initiation in the Wenchuan earthquake-stricken area,

southwestern China, Landslides, 11, 877-887, 2014.

Table 1. Characteristics of S-band Doppler weather radar.

Items	Value
Wavelength	10.4 cm
Polarized mode	horizontal
Antenna gain	45
First sidelobe level	-29 dBc
Peak transmitted power	750kW
Noise figure	4dB
Dynamic range	90dB
Range resolution	300m
Volume scanning elevation	0.5°, 1.5°, 2.4°, 3.4°, 4.3°, 6.0°, 9.5°, 14.5°, 19.5°
Altitude above sea level of radar location	595m for Chengdu site 557m for Mianyang site

Table 2. Characteristics of the rainfall events

Event No.	Date	Number of triggered debris flows	Event Duration by rain gauge (h)	Event Duration by radar (h)	Max. rainfall accumulation by rain gauge(mm)	Max. rainfall accumulation by radar(mm)
1	Jul. 9, 2012	9	12	11	17.5	29.6
2	Jul. 21, 2012	9	10	12	29.3	23.6
3	Aug.17–18, 2012	200	7	49	19.2	195.8
4	Jun. 19, 2013	15	5	12	55.3	101.8
5	Jul. 8-12, 2013	261	55	73	562.2	416.9
6	Jul. 10-12, 2014	25	20	21	28.5	17.8

Table 3. The comparison of radar rainguage for each estimate scenario

Criterions	Scenario I (Hybrid scan)			Scenario II (VPR)			Scenario III(Bias adjustment)		
	Region Type I	Region Type II	All study Region	Region Type I	Region Type II	All study Region	Region Type I	Region Type II	All study Region
NSE (%)	46.4	50	50.7	45.8	49.0	46.1	43.5	47.2	44.0
NMB (%)	-40.9	-42.8	-41.1	-17.1	-21.2	-18.6	1.7	10.8	1.91
CORR	0.80	0.77	0.78	0.82	0.77	0.80	0.85	0.82	0.84

Table 4. The parameters of Gaussian fitting which are used by frequentist method to account for I-D threshold

Parameters Of Gaussian fitting	Scenario I	Scenario II	Scenario III
a	3.144	2.55	2.22
b	0.011	0.003	-0.003
c	0.1273	0.1578	0.1868

Table 5. The metric for assessing the relative errors of the accumulated rainfall, duration and rainfall intensity versus distance

Factors	Rain gauge observation nearest to DF location versus Radar estimate at DF location	Radar estimate at the co-location of rain gauge versus Radar estimate at DF location
Accumulated Rainfall Relative Error (ARRE)	$ARRE_g(s) = \frac{\sum_{i=1}^{N(s)} \lvert R_{df}(i) - R_g(i) \rvert}{\sum_{i=1}^{N(s)} R_{df}(i)} \times 100\%$	$ARRE_r(s) = \frac{\sum_{i=1}^{N(s)} \lvert R_{df}(i) - R_r(i) \rvert}{\sum_{i=1}^{N(s)} R_{df}(i)} \times 100\%$
Duration Relative Error (DRE)	$DRE_g(s) = \frac{\sum_{i=1}^{N(s)} \lvert D_{df}(i) - D_g(i) \rvert}{\sum_{i=1}^{N(s)} D_{df}(i)} \times 100\%$	$DRE_r(s) = \frac{\sum_{i=1}^{N(s)} \lvert D_{df}(i) - D_r(i) \rvert}{\sum_{i=1}^{N(s)} D_{df}(i)} \times 100\%$
Rainfall Intensity Relative Error (RIRE)	$RIRE_g(s) = \frac{\sum_{i=1}^{N(s)} \lvert I_{df}(i) - I_g(i) \rvert}{\sum_{i=1}^{N(s)} I_{df}(i)} \times 100\%$	$RIRE_r(s) = \frac{\sum_{i=1}^{N(s)} \lvert I_{df}(i) - I_r(i) \rvert}{\sum_{i=1}^{N(s)} I_{df}(i)} \times 100\%$

Note. *R* represents accumulated rainfall for debris flow event, *D* represents duration for rainfall event, *I* represents the mean intensity for rainfall event. The variables with subscript df, g and r respectively represent the observation from radar at debris flow location, rain gauge nearest to debris flow location, and radar at the co-location of the nearest rain gauge. s represents the distance between the nearest rain gauge location and debris flow location with the range resolution of 300m. N(*s*) represent the number of rain gauge observation for debris flow at the distance of *s*.

Table 6. Parameters of the identified ID thresholds and relative errors

	α	$\frac{\alpha - \alpha_{S3}}{\alpha_{S3}} \times 100\%$	β	$\frac{\beta - \beta_{S3}}{\beta_{S3}} \times 100\%$
Scenario I	7.62	-24.5	0.67	28.8
Scenario II	8.7	-13.8	0.43	-17.3
Scenario III	10.1	0.0	0.52	0.0
Rain gauges	5.1	-49.5	0.42	-19.2
Radar estimate at the co-location of the nearest rain gauge	5.8	-42.6	0.41	-21.2

Note. α_{S3}, β_{S3} here equals to α, β estimated from Scenario III, respectively.

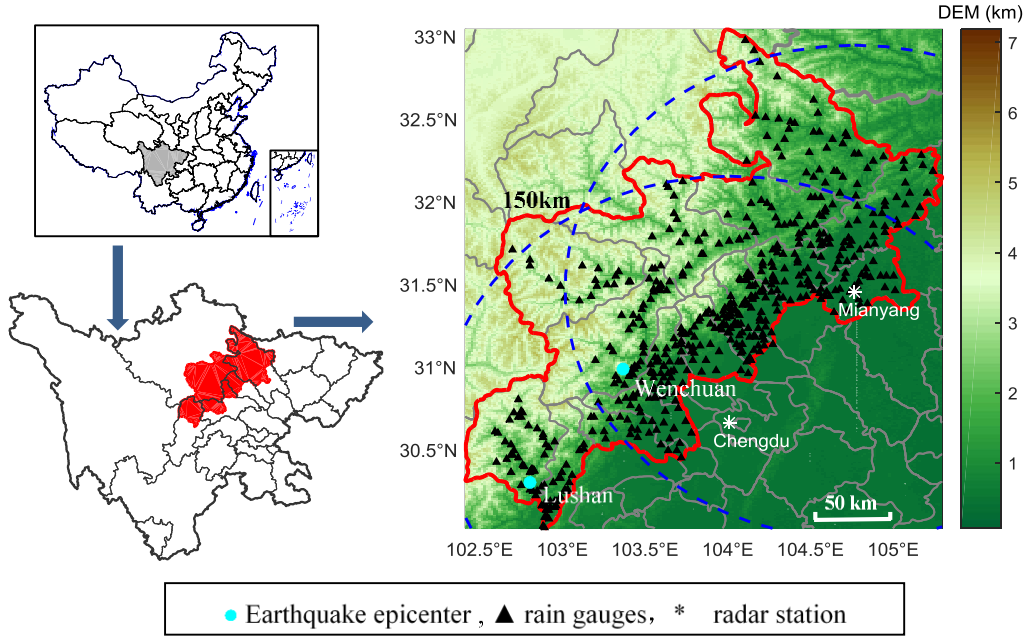

Figure 1. Location and Topography of the study area. Asterisk markers show the location of Chengdu and Mianyang S-band weather radar which respectively monitor the study area within 150 km (dash black circle) from radar location. Rain gauges in the study area are marked with black triangle and mostly deployed at the valley. The two blue circle dots are the epicentre of Ms8.0 Wenchuan earthquake in12th May , 2008 and Ms7.0 Lushan earthquake in20th April, 2013.

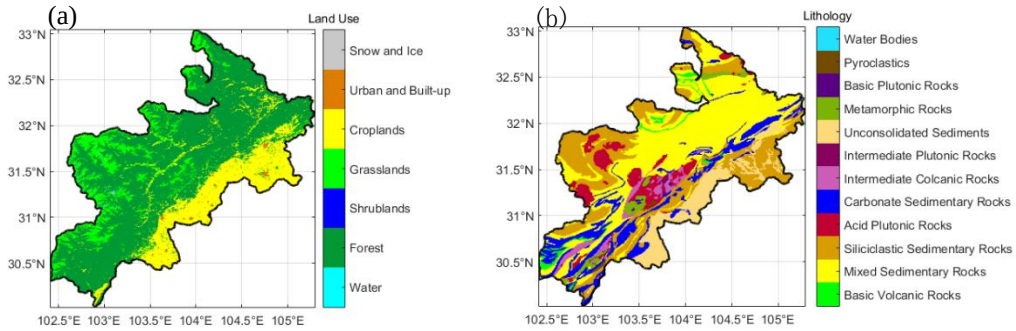

Figure 2. Lithology map (a) and land use map (b) for the study area

5

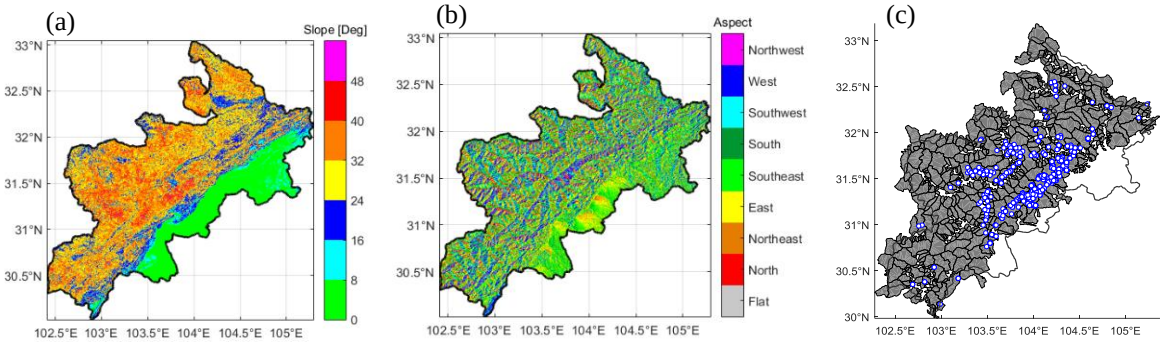

Figure 3. Morphology and potential DF watersheds map over study area.(a) slope, (b) aspect, (c) potential DF watersheds(gray polygon) with DF observation(blue circle)

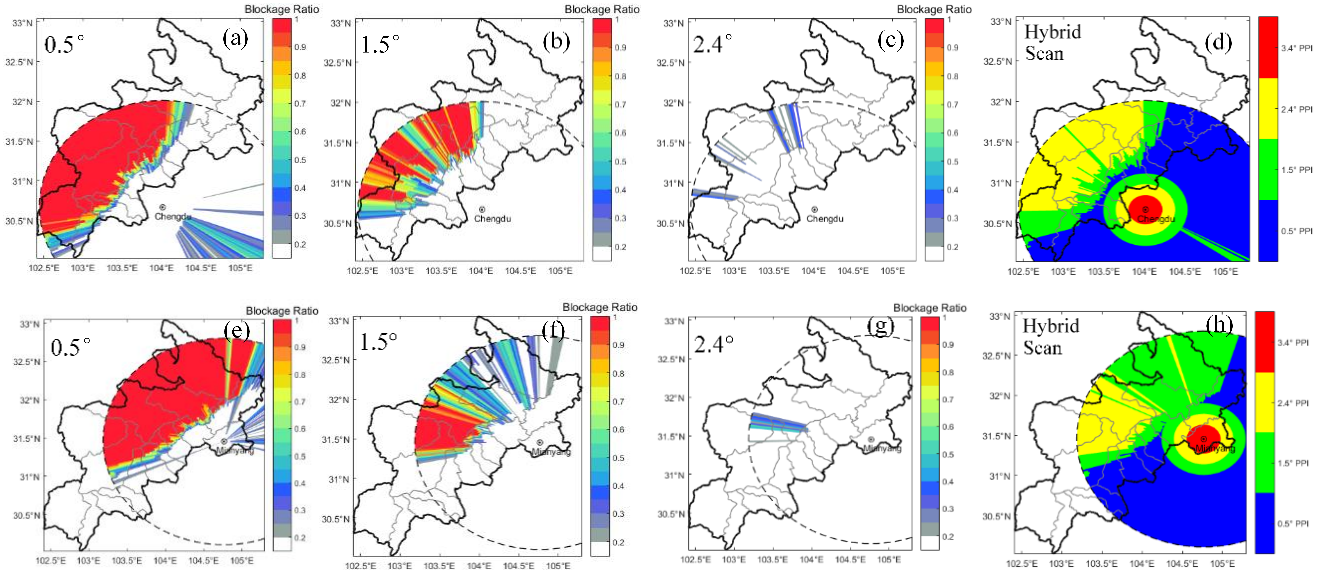

Figure 4. Blockage ratio of beam shielding for the radar main lobe beam and hybrid scan map. (a)-(c) represent the blockage ratio of Chengdu radar at the elevations of 0.5º, 1.5 º and 2.4 º respectively. (e)-(f) represent the blockage ratio of Mianyang radar at the elevations of 0.5º, 1.5 º and 2.4 º respectively. Hybrid scan maps for Chengdu and Mianyang are merged under the condition of blockage raito is lower than 0.5.

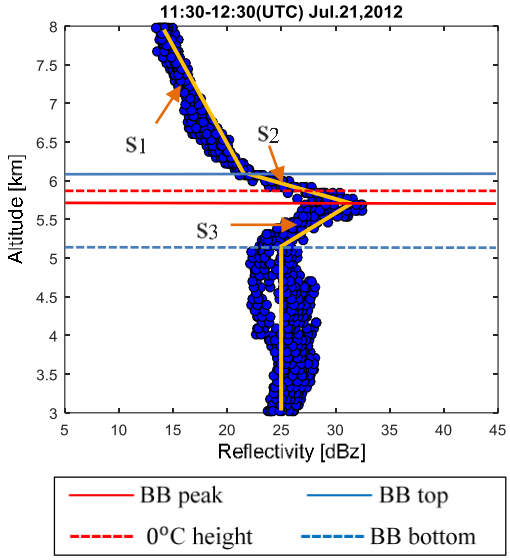

Figure 5. A real sample of VPR model processed in the study on Jul.21,2012. The Blue circle represents azimuthal mean of reflectivity over one hour. The orange line represents the idealized VPR with piecewise linear slope α,β, and γ. The horizontal blue lines is the bright band(BB) top and dashed blue lines is BB bottom. The solid red line and dashed red lines are BB peak and the 0°C height, respectively.

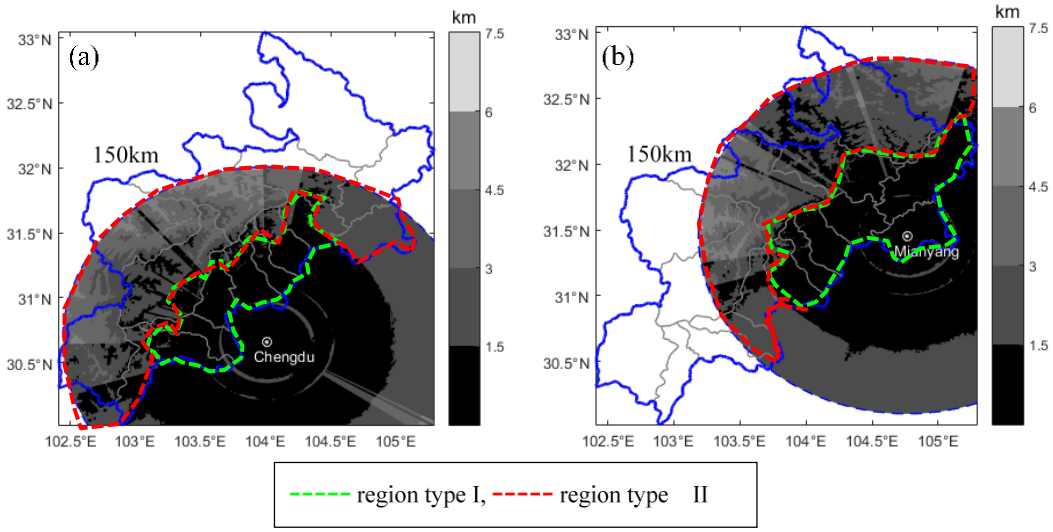

Figure 6.The height from the ground of hybrid scan for two S-band radar (a) radar located at Chengdu (b) radar located at Mianyang . The regions surrounded by green dash lines meet the condition of that the height from the ground is 1.5 km below and the distance from radar is inner 100 km and is recognized as region type I. The regions surrounded by the red dash lines represents the area under the opposite condition and is recognized as region type II.

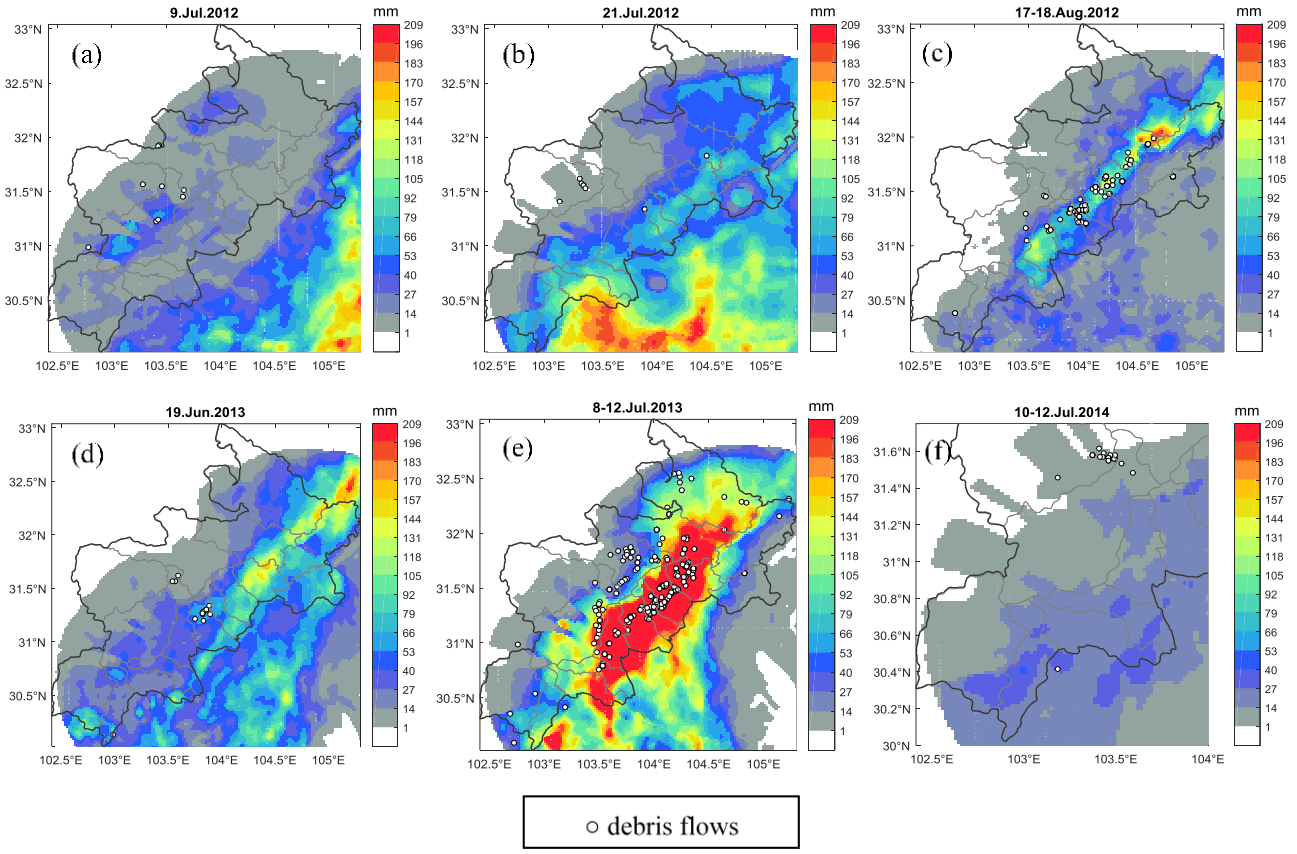

Figure 7. Images of radar-estimated rainfall accumulation for the six rainfall events (a–f). dotted circles represent the location of triggered debris flows. Events are showed in chronological order: (a) 9th July 2012; (b)21th July 2012; (c) 17-18th August 2012, (d)19th June 2013; (e)8-12th July 2013; (f)10th,12th July 2014.

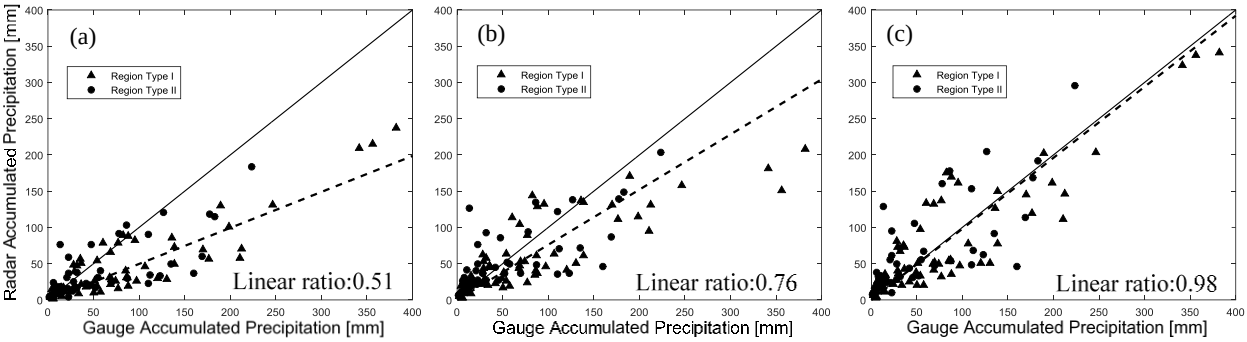

Figure 8. Scatter plots of radar and rain gauge event-rainfall accumulations. (a) Scenario1: radar estimate from hybrid scan. (b) Scenario 2: radar estimate from hybrid scan and VPR. (c) Scenario 3: radar estimate through the hybrid scan, VPR and bias correction.

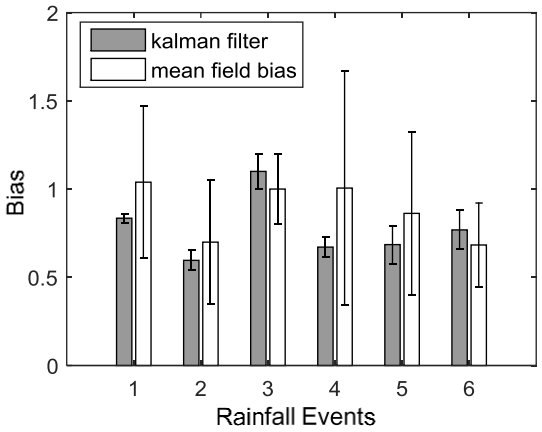

Figure 9. The average and covariance of bias estimation by Kalman filter and mean field bias method for six rainfall events.

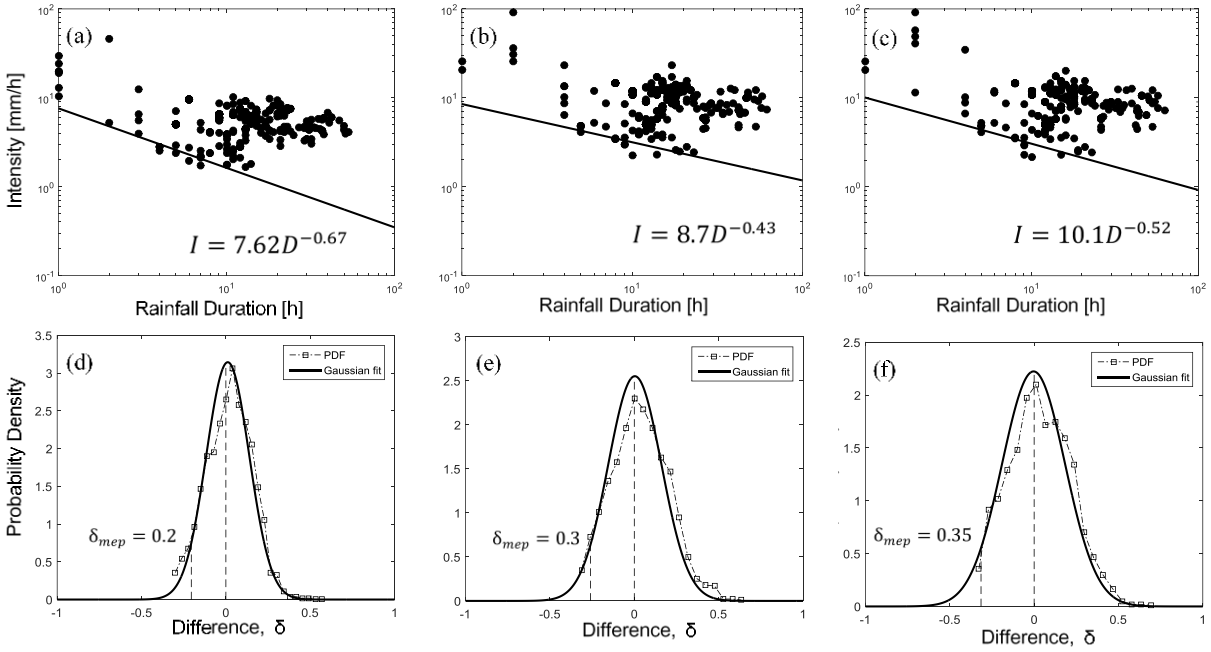

Figure 10. Scatter plots of radar and rain gauge event-rainfall accumulation and probability density function. (a), (b), (c) are the scatter plot of scenario I, II, III respectively.(d),(e) and (f) are the Gaussian fitted PDF of scenario I, II, III respectively.

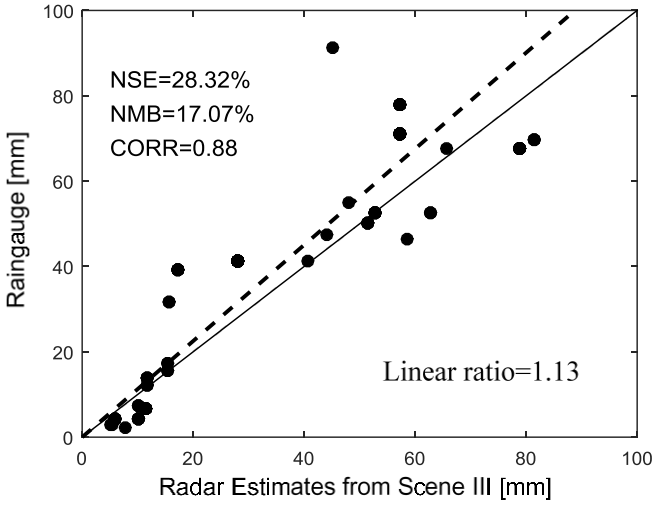

Figure 11. Event-rainfall scatter plots of rain gauges nearest to debris flow locations and radar-based estimate from scenario III over the same location of rain gauge.

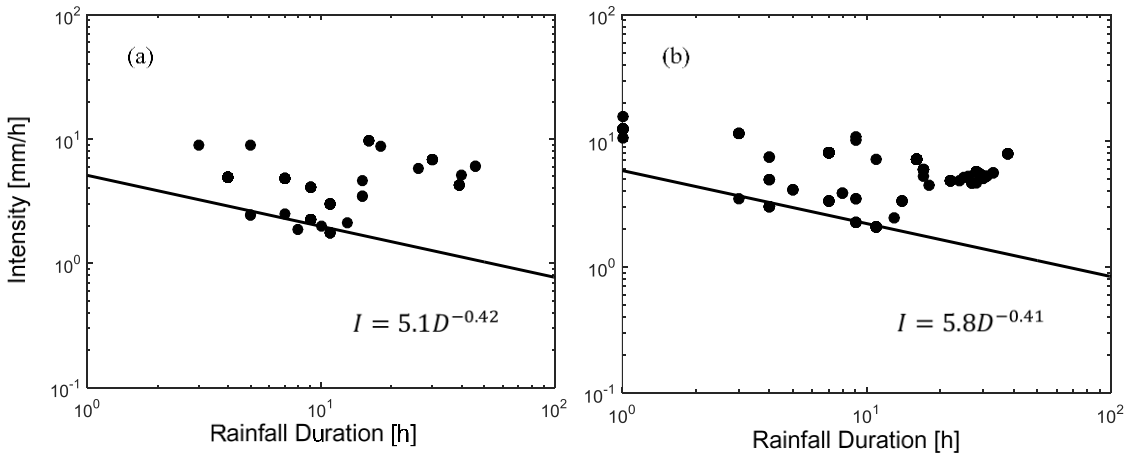

Figure 12. Intensity–duration thresholds (black line) derived from (a) rain gauges nearest to debris flow locations and (b) radar rainfall estimation at the same location of the rain gauges nearest to the debris flow.

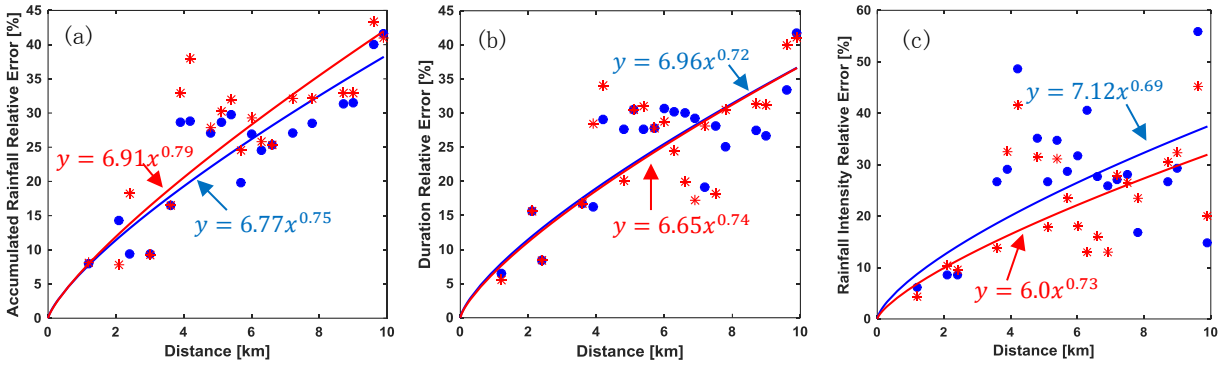

Figure 13. Scatterplot of relative errors versus distance. Blue circle dot represent relative error between radar estimate at debris flow location and rain gauge observation nearest to debris flow location. Red asterisk represent relative error between radar estimate at debris flow location and radar estimate at the co-location of the nearest rain gauge.(a) Accumulated Rainfall Relative Error(ARRE), (b) Duration Relative Error (DRE), (c) Rainfall Intensity Relative Error (RIRE).

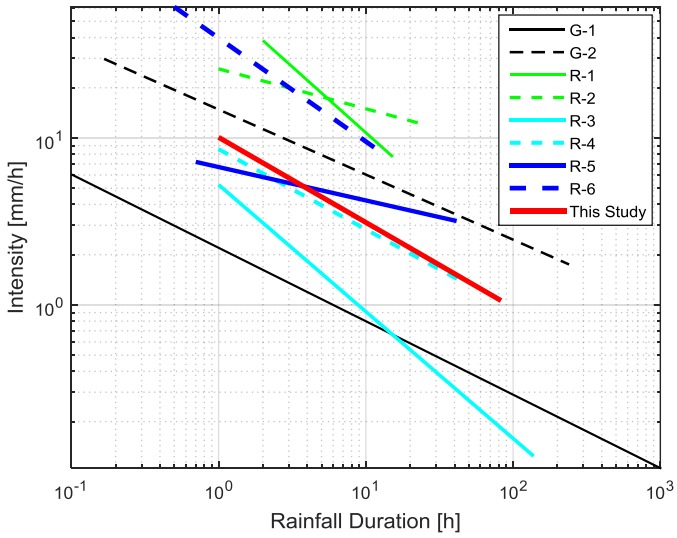

Figure 14. I–D thresholds determined for this study (red line) and those of various other studies. G = global,R = region. G-1: Guzzetti et al. (2008); G-2: Caine (1980); R-1: Wenchuan earthquake area, Wei and Tang(2014); R-2: Qingping, a region in Wenchuan earthquake area, Tang et al. (2012); R-3: Wenchuan earthquake area, Xiaojun G. et al.(2016); R-4:Italy, Francesco M. et al.(2014); R-5 Central Taiwan, Jan and Chen(2005);R-6 Japan, Jibson (1989).